SEMMELWEIS EGYETEM

DOKTORI ISKOLA

Ph.D. értekezések

3301.

BUI DÁVID

Funkcionális Idegtudományok

című program

Programvezető: Dr. Sperlágh Beáta, egyetemi tanár

Témavezető: Dr. Christos Chinopoulos, egyetemi docens

MITOCHONDRIAL SUBSTRATE-LEVEL PHOSPHORYLATION: FROM METABOLIC INTERFERENCE TO SMALL MOLECULE INTERACTIONS

PhD thesis

Dávid Bui

Semmelweis University Doctoral School

János Szentágothai Neurosciences Division

Supervisor: Dr. Chinopoulos Christos, MD, D.Sc

Official reviewers: Dr. Gallyas Ferenc, D.Sc
Dr. Kardon Tamás, MD, Ph.D

Head of the Complex Examination Committee: Dr. Rónai Zsolt, MD, D.Sc

Members of the Complex Examination Committee: Dr. Sarnyai Farkas, Ph.D
Dr. Gallyas Ferenc, D.Sc

Budapest
2025

Table of Contents

List of Abbreviations

ADP ..... adenosine 5’-diphosphate

Ala ..... alanine

anox ..... anoxia

ANT ..... adenine nucleotide translocase

Asn ..... asparagine

ATP ..... adenosine 5’-triphosphate

atpn ..... atpenin A5

bHB ..... β-hydroxybutyrate; 3-hydroxybutyrate

BSA ..... bovine serum albumin

cATR ..... carboxyatractyloside

CoA ..... coenzyme A

complex I ..... NADH:ubiquinone oxidoreductase

COX ..... cytochrome c oxidase

DCPIP 2,6-dichlorophenolindophenol; 2,6-dichloroindophenol

DNA ..... deoxyribonucleic acid

DTNB ..... 5,5′-dithiobis-(2-nitrobenzoic acid)

DTT ..... dithiothreitol

EDTA ..... ethylenediaminetetraacetic acid

EGTA ..... 3,12-bis(carboxymethyl)-6,9-dioxa-3,12-diazatetradecane-1,14-dioic acid

FEP ..... fluorinated ethylene propylene

GC-MS ..... gas chromatography coupled to mass spectrometry detection

G3P sn-glycerol-3-phosphate; D-glycerol-1-phosphate

glut ..... glutamate

GTP ..... guanosine 5’-triphosphate

HEPES ..... 2-[4-(2-hydroxyethyl)piperazin-1-yl]ethane-1-sulfonic acid

H_2O_2 ..... hydrogen peroxide

IMAC ..... immobilized metal affinity chromatography

IMM ..... inner mitochondrial membrane

KGDHC ..... 2-oxoglutarate dehydrogenase complex

LED ..... light-emitting diode

Leu ..... leucine

Ly266500 ..... 2-(3-chloro-4-fluorophenyl)-3(2H)-isothiazolone

mal ..... malate

MDH2 ..... mitochondrial malate dehydrogenase, mitochondrial

Met ..... methionine

mito ..... mitochondria

Mw ..... molecular weight

NAD ..... nicotinamide adenine dinucliotide

NADH ..... reduced nicotinamide adenine dinucleotide

$[O_2]$ ..... oxygen concentration

$-\Delta[O_2]/\Delta t$ ..... oxygen-consumption rate

PAGE ..... polyacrylamide gel electrophoresis

PCR ..... polymerase chain reaction

PVDF ..... polyvinylidene difluoride

rot ..... rotenone

SDH ..... succinate dehydrogenase

SDS ..... sodium dodecyl sulfate

Ser ..... serine

SF ..... SF-6847; 2-[(3,5-ditert-butyl-4-hydroxyphenyl)methylidene]propanedinitrile

STK ..... succinate thiokinase; succinate-CoA ligase

succ ..... succinate

Thr ..... threonine

Tris ..... 2-amino-2-(hydroxymethyl)propane-1,3-diol; tris(hydroxymethyl)aminomethane

UV ..... ultraviolet

Val ..... valine

1. Introduction

In eukaryotic cell, mitochondria are compartmentalized hubs of primary metabolism. Carbohydrate, amino acid, isoprene and fatty acid metabolic pathways both end and start from them. Mitochondria's ability to perform their role in the cell is also tightly intertwined with cellular respiration owing to the mitochondrial electron transport chain. Consequently, oxygen deprivation has a direct and immediate effect on mitochondrial processes. Hypoxic conditions may be found in solid tumours far from sufficient vasculature (1, 2), in various pathological ischemic conditions (3) or even in physiological niches (4). For example, hepatocellular carcinomas (5), prostate cancer (6), cervical carcinomas (7), head and neck carcinomas (8) have all been characterized to have variable extent of hypoxic regions, and even in some cases of leukaemia, hypoxia in bone marrow plays a role (9). Tumour hypoxia has been negatively correlated to patient prognosis and treatment responsiveness (10). Many cancers acquire metabolic adaptations to hypoxic environments, which they retain even with adequate oxygen supply as a selective advantage (2), a pseudo-hypoxic metabolism phenotype. One of the main regulators involved is hypoxia-inducible factor 1 (11), which, when stabilized, causes a variety of transcriptional changes related to metabolism. Stimulates the expression of glucose transporters, glycolytic enzymes and lactate dehydrogenase, restricts pyruvate dehydrogenase through increased pyruvate dehydrogenase kinase expression and shifts the cytochrome c oxidase subunit COX4 from the COX4-1 to the COX4-2 isoform (12). Physiologically, it is highly variable and questionable whether glycolysis or oxidative phosphorylation serves as the main source of ATP (13). However, under hypoxic conditions, cytosolic glycolysis will increasingly become the more important energy source (3, 14). Mitochondria, on the other hand, must maintain a delicate balance between ATP availability and membrane potential. Mitochondrial membrane potential across the inner membrane is a key functional parameter of the organelle regardless of the disease (15). Until approximately 0.8 μM (80 Pa) oxygen concentration, over half of cytochrome c oxidase activity is retained (16, 17), and the respiratory chain can maintain the membrane potential. For comparison, normal oxygen tension in the brain cortex is around 44-64 μM (18, 19), with values below 27 μM negatively correlated to survival after brain injury (20), and less than 13 μM manifesting in ATP depletion (21). On the other hand,

values as low as 9 μM in white matter and 1.5 μM in the fornix have also been reported (22). Cell-body-dense regions usually have better oxygenation than fibrous areas (23). In more severe hypoxia, however, considering the reversibility of both the adenine nucleotide translocator (ANT) and the ATP synthase becomes crucially important (24, 25). Once mitochondria cannot maintain their membrane potential using the energy of electron transfer reactions, ATP synthase would start expending the energy available in ATP and act as a hydrogen ion pump, since that becomes energetically more favourable (26). This would decrease the ATP/ADP ratio in the mitochondrial matrix in comparison to the cytosol, which would act as a driving force for ANT to facilitate the transport of ATP into mitochondria. There is an endogenous protein, called "inhibitory factor 1" that can act as an inhibitor of hydrolysis by ATP synthase under certain conditions, such as acidic pH or loss of membrane potential (27). The amount of inhibitory factor 1 expressed in different cells relative to ATP synthase was found to be variable in different tissues (28), but it was overexpressed in some cancers (29, 30). By inhibiting the ATP synthase, cells can preserve ATP, however, it comes at the cost of rapid mitochondrial depolarisation (27). This could impair normal membrane-potential-dependent mitochondrial functions, such as ion homeostasis (31), metabolite transport (32) or protein import (33) and may lead to the elimination of mitochondria (34). The energetic dependence on cytosolic ATP can be prevented if another substrate-level process provides the membrane potential and/or the ATP in the mitochondrial matrix (35). The mitochondrial substrate-level phosphorylation by the citric acid cycle enzyme succinate-CoA ligase (STK) is the primary candidate for this role. STK can use the chemical energy in the thioester bond to phosphorylate ADP into ATP through the intermediate phosphorylation of an active site histidine residue. The enzyme is a heterodimer and has both ATP- and GTP-specific forms, depending on the beta subunit (36).

In our theory, STK is the key enzyme that provides the small amount of ATP required inside mitochondria to prevent the import from the cytosol (35). Intervening in this enzyme's function is a way to specifically target cells that rely on substrate-level phosphorylation for bioenergetics. For example, either fostering growth of embryonic cells, or killing cancerous cells. The most limiting factor for the chemical energy transmission is the availability of mitochondrial succinyl-CoA supply.

2-oxoglutarate dehydrogenase (KGDHC) is likely the greatest and most accessible provider of succinyl-CoA (37). Glutamine, glutamate, and to a much lesser extent 2-oxoglutarate are available from blood supply (38-41). Proline, histidine and ornithine could also contribute, but their metabolism takes several additional steps and in the case of proline and ornithine, an additional oxidation step by delta-1-pyrroline-5-carboxylate dehydrogenase is also required (42). Histidine on the other hand is an essential amino acid, therefore it is more valuable for purposes other than ATP synthesis (43). Glutamine is by far the most widely available amino acid and the hydrolytic cleavage of the amide group provides glutamate without additional reductive burden. In transformed cells, enhanced glutaminolysis (the use of glutamine catabolism for citric acid cycle anaplerosis or energy generation) has been one of the characteristic metabolic phenotypes (44, 45). Glutamate is converted to 2-oxoglutarate either by transamination or by glutamate dehydrogenase. Glutamate is one of the central players in organic nitrogen metabolism, because many different transaminases use the glutamate – 2-oxoglutarate couple as co-substrates for the carbonyl – amine group exchange (46). Related to this, glutamate dehydrogenase is the enzyme facilitating the disposal of nitrogen from the carbon chain alongside an electron pair transfer to NAD or NADP (47). The 2-oxoglutarate with the use of NAD and CoA can then be oxidised further by KGDHC to produce the thioester-bond-carrying succinyl-CoA (48). *In vitro*, glutamate catabolism with isolated mitochondria results in high oxygen consumption rates, indicating the availability of associated enzymes at high capacity. A major hindrance for KGDHC during hypoxia comes from the availability of NAD. This reducing equivalent carrier coenzyme relies on regeneration by complex I (NADH:ubiquinone oxidoreductase) and the electron transport chain under normal circumstances. However, in hypoxia this is no longer possible, and anything affecting the NAD/NADH ratio can indirectly alter the rate of mitochondrial substrate-level phosphorylation. This was demonstrated for example in the case of NQO1 (49), an enzyme capable of oxidising NADH by reducing quinoidal compounds.

2. Objectives

2.1 Substrate-level phosphorylation with 2-oxobutyrate

Alternative to 2-oxoglutarate, 2-oxobutyrate is another oxocarboxylic acid that can be converted to mitochondrial succinyl-CoA. 2-oxobutyrate is first oxidised to propionyl-CoA (50) with the reduction of a NAD. Propionyl-CoA is then carboxylated to (S)-methylmalonyl-CoA (51) using one equivalent of ATP for the carbon dioxide activation. Through two energetically neutral isomerisation steps, (S)-methylmalonyl-CoA becomes succinyl-CoA (52). Overall, the pathway to succinyl-CoA from 2-oxobutyrate is energetically very similar to that from 2-oxoglutarate, except for the additional carboxylation step, which uses up an additional ATP per molecule. This ATP expenditure cancels out the energy yield of the substrate-level phosphorylation step. In total, 2-oxobutyrate gives no net ATP, while 2-oxoglutarate gives 1 ATP. We sought to investigate the interaction between the two pathways, especially when mitochondria are dependent on the ATP made by substrate-level phosphorylation.

2.2 Promoting KGDHC operation in anoxia

1. We searched for various possibilities that can overcome the NAD limitation of KDGHC under hypoxic conditions and support substrate-level phosphorylation. This means, either finding an alternative electron acceptor, or regenerating NAD at the substrate-level by coupling it to another enzyme's activity. Similar to how lactate dehydrogenase regenerates cytosolic NAD in fermentative glycolysis. Generally, NADH exerts a strong driving force derived from its highly negative reduction potential (53) in the direction of the associated substrate reduction (54, 55). For example, under physiological conditions, malate dehydrogenase (MDH2) needs the oxaloacetate concentration to be kept low by citrate synthase to promote the malate-to-oxaloacetate direction over the reverse (55). Weinberg et al. showed that the combination of 2-oxoglutarate and aspartate was able to mitigate hypoxia-reperfusion-associated damage by reductive MDH2 and succinate dehydrogenase (SDH) operation (56). We tested whether MDH2 alone, without SDH would also be sufficient to support substrate-level phosphorylation (Fig. 1).

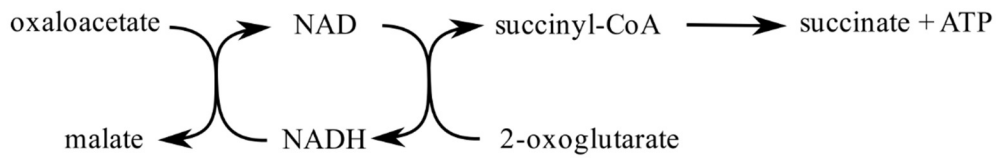

Figure 1, A scheme showing the hypothetical contribution of MDH2 to substrate-level phosphorylation.

2. Similarly, if SDH can reduce fumarate in its reverse direction, then coupled through ubiquinone, complex I could continue its function as the NAD regenerator, but would be driven by an electron acceptor metabolite instead of relying on cytochrome c oxidase. This idea has been proposed in the past (57, 58) and there are empirical observations of succinate accumulation under oxygen limited conditions in animals (59). However, mammalian SDH is also known to have a diode-like behaviour (60). When the reaction rate is measured as the function of applied potential, succinate oxidation increases proportionally, but fumarate reduction sharply decreases after a maximum point. In steady-state experiments using reduced benzyl viologen (a reducing agent), the fumarate reduction rate is around 40 times less than succinate oxidation (61, 62). Still, the reaction rate towards succinate is not zero and even a low rate could be sufficient to support substrate-level phosphorylation (Fig. 2). Commonly, mitochondrial experiments use substrate combinations that include malate to facilitate the co-transport or as an anaplerotic auxiliary substrate. However, malate and fumarate are easily interconverted by mitochondrial fumarase, with only a small preference for the fumarate-to-malate direction (63). So, we sought to investigate whether succinate dehydrogenase reversal occurs under our experimental conditions.

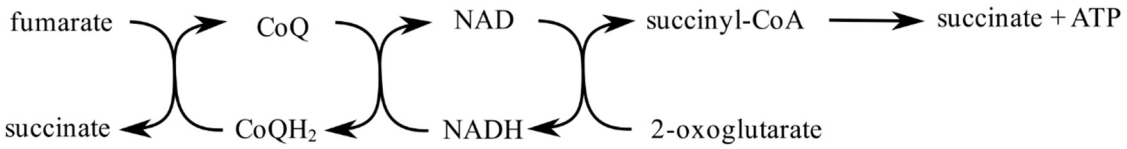

Figure 2, A scheme showing the hypothetical contribution of SDH to substrate-level phosphorylation.

3. We also thought about addressing the possibility that the membrane potential indicator dye safranin, which has been used by the group for a long time, could also act as an electron acceptor. Safranin has a phenazine structure like that of N-methyl-phenazonium and N-ethyl-phenazonium. The latter two are known mediators for electron

transfer from NADH to other compounds, like various tetrazoliums (64). There is also literature about the electrochemical properties of safranin (65-67), and it was used as a mediator in potentiometric titrations (68, 69). In addition, it also has known adverse effects on mitochondrial function (70-73). At a glance, safranin's structure is also very similar to that of triphenyltetrazolium, which was shown to get reduced by complex I under anoxic conditions (74). Methylene blue, a dye from a different compound family, is known to react with NADH, ubiquinone and oxygen (75, 76), and was shown to promote mitochondrial substrate-level phosphorylation under rotenone inhibition (77). The core 3,7-diaminophenotiazin-5-ium structure of methylene blue is very similar to safranin's 3,7-diaminophenazin-5-ium structure, the only difference is the nitrogen atom in the place of the sulphur atom. All these similarities raise the suspicion that safranin can also act as an electron acceptor. To our knowledge, nothing regarding electron transfer interactions of safranin with mitochondria has been published so far, therefore we sought to investigate the possibility, and if we do find an interaction, to characterise it.

2.3 Direct STK inhibition

Having an inhibitor for STK would be useful to directly and unambiguously address the importance of STK's contribution to the bioenergetic balance. By inhibiting the enzyme, we could also address viability alterations in model cell cultures under specific, pathological experimental conditions. A systematic search for a new inhibitor has been out of reach for smaller research groups in the past due to the resources required for screening large compound libraries compound-by-compound in order to identify promising candidates (78). However, the development of DNA-encoded libraries now allows the rapid parallel screening of large numbers of molecules based on their relative binding affinity to the target, which simplifies the process (79). Binding does not necessarily mean inhibition, but without binding there is no inhibition. The principle behind this approach is the use of DNA as a known barcode, which is covalently attached to either a molecule with numerous surface features or a smaller molecule fragment presenting only one or a few binding groups. The strength of the method is that any number of these can be mixed together, as long as their DNA sequences are unique. For an identification sequence with *n* base pairs, up to 4^n unique sequence-molecule couples can be used simultaneously in one mixture. However, in practice, because the libraries are synthesised block-by-block, barcoding is much less efficient. The DNA sequences

corresponding to the molecules with the highest relative binding affinity to the target can then be amplified with polymerase chain reaction (PCR) sequenced and identified based on their reading frequency.

For this, first we need to produce the enzyme in sufficient quality and quantity, and make sure it is stable and functional. Due to limitations, only the ATP-specific, phosphorylated form of the human STK was chosen for screening. Afterwards, we need to validate the inhibitory properties of our best hits.

The objectives are summarized in Fig. 3.

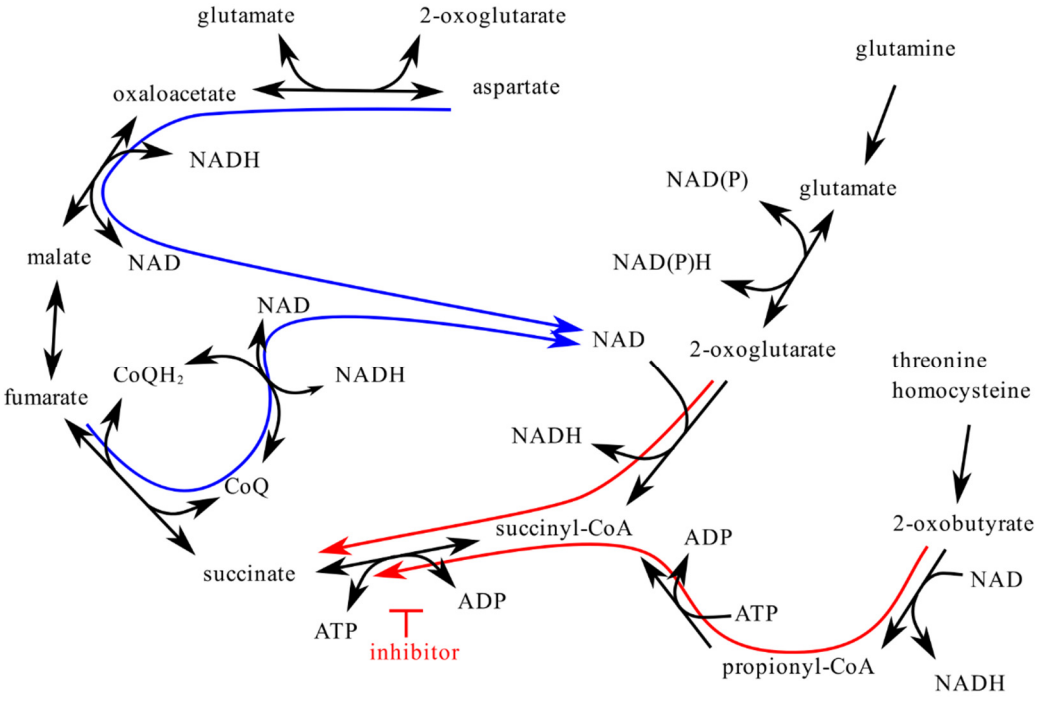

Figure 3, A schematic summary of the metabolite pathways along with their notable co-substrates/coenzymes. Coloured arrows are highlighting the most important routes with respect to the dissertation: blue arrows are indicating the chain of electron acceptors for NAD provision; red arrows are indicating the pathways towards mitochondrial substrate-level phosphorylation.

3. Methods

Animals

Mice were of mixed 129 Sv and C57Bl/6 background. The animals used in our study were of either sex and between 2 and 6 months of age. Data obtained from liver mitochondria of mice of a particular gender or age (2, 4 or 6 months) did not yield any qualitative differences, thus all data were pooled. Mice were housed in a room maintained at 20–22°C on a 12-h light–dark cycle with food and water available ad libitum. All experiments were in accordance with the guidelines of the Semmelweis University Workplace Animal Welfare Body Committee.

Isolation of mitochondria

Liver and brain mitochondria were isolated as described in (37) with the following modifications. The centrifugation sequence for liver mitochondria was 700 g ($r_{average}$) for 10 min; followed by two times 7850 g for 10 min and mitochondria was suspended in 0.1 ml solution per mouse. The centrifugation sequence for brain mitochondria was 700 g for 10 min, 7850 g for 10 min, 29000 g for 6 min, 15750 g for 10 min, 7850 g for 10 min and mitochondria was suspended in 25 µl per mouse of the same solution used for liver mitochondria. Protein concentration was determined using the bicinchoninic acid assay and calibrated using bovine serum albumin standards (80) using a Tecan Infinite® 200 PRO series plate reader (Tecan Deutschland GmbH, Crailsheim, Germany).

Determination of membrane potential in isolated mitochondria

Membrane potential of isolated mitochondria (0.5 mg for mouse liver and 0.25 mg for brain per 2 ml of medium) was estimated fluorimetrically with 5 µM safranine(81), acknowledging the considerations elaborated in (73, 82) regarding inhibition of respiration as well as unspecific binding of safranine. Fluorescence was recorded in a Hitachi F-7000 spectrofluorimeter (Hitachi High Technologies, Maidenhead, UK) at a 5-Hz acquisition rate, using 495- and 585-nm excitation and emission wavelengths, respectively with 20 nm bandwidth. Experiments were performed at 37°C in 8 mM KCl, 110 mM K-gluconate, 10 mM NaCl, 10 mM HEPES, 10 mM K_2HPO_4, 0.01 mM EGTA,

10 mM mannitol, 1 mM $MgCl_2$, 0.5 g/l BSA, pH adjusted to 7.25 with KOH unless stated otherwise.

Simultaneous fluorescence and oxygen concentration measurement

Membrane potential for 0.5 g/l liver mitochondria was estimated fluorimetrically in an enclosed 2 ml volume with 5 µM safranin or rhodamine 123. Fluorescence was recorded in an Oxygraph-2k or a NextGen-O2k at a 0.5-Hz acquisition rate, using a 465 nm LED with a 550 nm short-pass excitation filter and a photodiode with a 570 nm long-pass emission filter. For both dyes, decreasing fluorescence means increasing membrane polarisation (in absolute value) due to quenching.

At the same time, oxygen concentration was monitored amperometrically using a Clark electrode separated by a 25 µm FEP membrane from the bulk solution.

Electrochemical measurements

Voltammetric measurements were made with the Q-Module of the NextGen-O2k. This is made up of a glassy carbon working, a platinum auxiliary and a Ag/AgCl reference electrode. The applied potential difference between the working and reference electrodes is controlled by the DatLab software. All potentials are reported versus the secondary Ag/AgCl reference (with 3 M KCl). The concentrations of reduced ubiquinone-2 and reduced safranin were measured with amperometry. The constant electrode polarisation was set to either 30 mV or -100 mV. 30 mV was only used when ubiquinone was measured. For safranin there was no difference between the results at the two polarisations. At these potentials, the measured current is limited by the electron transfer step between the electrode surface and the compounds in the solution. Decreasing negative current means a higher concentration of reduced compounds.

Targeted metabolite GC-MS

Mitochondrial suspensions were 'spiked' with 1 mM L-norleucine, a non-metabolizable substrate that yields a highly recognizable signature during the metabolite analysis and was used for normalizing volumes and keeping pipetting errors at check. Experiments were started with 5 mM malate and 2.5 mM glutamate as initial respiratory substrates. After adding 1 mg mitochondria and 2mM ADP, at approximately 10 µM oxygen concentration, 2.5 mM glutamate-$^{13}C_5$ was added. At 76 s, 276 s or 676 s after glutamate-

$^{13}C_5$ addition, an inhibitor cocktail (1 µM rotenone, 0.5 mM N-ethylmaleimide, 1 µM atpenin, 1 µM myxothiazole, 1 mM arsenite, 0.1 mM p-hydroxymercurybenzoate, 0.1 mM aminooxyacetic acid, 1 mM cyanide) was added and immediately three 0.6 ml aliquots from the 2 ml mitochondrial suspensions were spun at 14,000 rpm for 5 min at 4°C. Any visible aqueous phase was removed from the pellets and discarded. To each tube 0.5 ml of ice-cold 80 v/v% methanol was added. The tubes were frozen and kept in −80°C until further processing. Later, proteins, particulates and lipids were removed by chloroform extraction and centrifugation. The aqueous phase was evaporated to dryness with a centrifugal evaporator. Once dry, the dried lysates were stored at − 80°C until further analysis. Dried lysates were derivatized using a two-step protocol. Samples were first treated with 2% methoxyamine in pyridine (40 µl, 1 h at 60°C), followed by addition of N-(tertbutyldimethylsilyl)-N-methyl-trifluoroacetamide, with 1% tert-butyldimethyl-chlorosilan (50 µl, 1 h at 60°C). Samples were transferred to glass vials for GC–MS analysis using an Agilent 8890 GC and 5977B MSD system. 1 µl of sample was injected in splitless mode with helium carrier gas at a rate of 1.0 ml·min^{-1}. Initial GC oven temperature was held at 100°C for 1 min before ramping to 160°C at a rate of 10°C·min^{-1}, followed by a ramp to 200°C at a rate of 5°C·min^{-1} and a final ramp to 320°C at a rate of 10°C·min^{-1} with a 5 min hold. Compound detection was carried out in scan mode. Total ion counts of each metabolite were normalized to the internal standard norleucine.

Hydrogen peroxide measurement

The wavelength dependence of the photoinduced reaction was determined by measuring indirect hydrogen peroxide production. Separate solutions containing 5 µM safranin, 0.25 mM NADH in 50 mM pH 7.2 phosphate buffer were exposed to light irradiation at 25 nm intervals with 20 nm bandwidth for 10 minutes. A sample aliquot from each was acidified with 5 M H_2SO_4 to approximately pH 2-3 and stored on ice. After the final sample was taken, all samples were taken to room temperature for 15 minutes to degrade excess NADH. Smaller aliquots of the samples were neutralized with a Tris solution, followed by the addition of 30 µM Amplex UltraRed and 20 mg/l horseradish peroxidase. The absorbance of the resulting Amplex UltroxRed was then measured at 565 nm.

Recombinant STK expression

Transformed BL21(DE3) Escherichia coli were grown to a density of 0.4-0.6 OD_{600} at 37°C in Lennox type broth with 30 mg/l kanamycin. Following induction with 0.1 mM isopropyl β-D-1-thiogalactopyranoside, bacteria were left to express proteins overnight for approx. 16-20 hours at 20°C. Bacteria were collected with centrifugation and frozen for later use. Pellet was suspended in approx. 10 ml per g wet weight in the lysis solution (50 mM NaH_2PO_4, 0.3 M NaCl, 10 mM imidazole, 10 w/v% glycerol, pH 8.0) with added 0.2 mM phenylmethylsulfonyl fluoride and 3 mM DTT. Cell contents were liberated with 1 s sonication every 2 s for 6 min at 80% amplitude. Cell debris was removed with centrifugation and filtration through a 0.22 μm PVDF membrane filter. The filtrate was then applied to a Ni-IMAC (EDTA-compatible) gravity column, washed with 20 mM imidazole and eluted with 100 mM imidazole. The rest of the solution composition was the same as for the lysis. To the eluate, 10 mM DTT was added, and the bulk solution was changed to a solution containing 20 mM imidazole, 50 mM NaCl, 10 w/v% glycerol, pH 7.2 by ultrafiltration with a 10000 Mw cut-off Amicon tube. After concentration, the protein was passed through a Q-Sepharose anion-exchange gravity column in negative mode and 3 column volumes of flow-through were collected. To the collected volume 5 mM DTT was added and then exchanged with the Step-Tactin binding solution (100 mM Tris, 150 mM NaCl, 1 mM EDTA, 3 w/v% glycerol, pH 7.3). The preparation was stored overnight at 4°C with 1 mM ATP and 6 mM $MgCl_2$ added. Then, the preparation was applied to a StrepTrapXT column, washed with the binding solution and eluted with 50 mM biotin (in the same solution). 1 mM DTT was added to the eluate and exchanged for the storage solution (50 mM Tris, 20 w/v% glycerol, pH 7.5) before aliquoting and freezing. Concentration was measured with UV absorbance in a 1 cm cuvette $A_{0.1\%}$ = 0.442 at 278 nm (calculated from amino acid composition) corrected for light scattering at 330 nm.

STK activity assay

Thioester bond formation $\Delta\varepsilon = 4.5\ mM^{-1}cm^{-1}$ was followed at 232 nm 25°C in a solution containing 50 mM Tris pH 7.6, 10 mM succinate, 5 mM $MgCl_2$, 0.2 mM ATP, 0.2 mM CoA. The maximal reaction rate at the inflection point was used to represent enzymatic activity.

For measurements with immobilised enzyme, the excess CoA was detected with 62.5 µM DTNB after reaction in a mixture of 5.3 mM succinate, 0.1 mM ATP, 1 mM $MgCl_2$, 21 µM CoA, 10 mM Tris, pH 8.0.

Polyacrylamide gel electrophoresis

Standard Laemmli (83) composition system was used. Stacking gel with 0.1 w/v% SDS, 5 w/v% acrylamide mixture (2.6% methylenebisacrylamide), 125 mM Tris, pH 6.8. Resolving gel 0.1 w/v% SDS, pH 8.8, 10 w/v% acrylamide mixture (2.6% methylenebisacrylamide), 375 mM Tris. Running solution was 0.1 w/v% SDS, 25 mM Tris, 192 mM glycine with 150 V direct current applied for 60-65 minutes. For native PAGE, SDS was omitted, and acrylamide concentration was reduced to 3 w/v% for stacking and 6 w/v% for resolving gel.

Samples were prepared with NuPAGE LDS Sample Buffer (4X) and 50 mM DTT, and heated for 10 min at 70°C. If the sample contained significant amounts of imidazole, heating was reduced to 5 min at 37°C.

Gels were stained with 0.25 w/v% Coomassie brilliant blue R-250, 10 v/v% acetic acid, 45 v/v% ethanol, 45 v/v% water. Excess dye was removed with 10 v/v% acetic acid, 25 v/v% ethanol, 65 v/v% water.

DNA-encoded library screening and DNA sequencing

The enzyme was bound to magnetic Ni-IMAC beads in 50 mM NaH_2PO_4, 0.1 M NaCl, 10 w/v% glycerol, pH 7.4. The excess was washed off with added 0.05 w/v% polysorbate 20. Then the library was allowed to bind to blank beads or beads with the enzyme in the presence of 10 mg/l herring sperm DNA non-specific blocker at 4°C for 2 hours with continuous mixing. Following washing, the bound enzymes and compounds were eluted with 360 mM imidazole. The eluate was then frozen. DNA labels were amplified and elongated with PCR. The settings and primers were specified by the manufacturer. PCR products were purified with agarose gel electrophoresis and gel extraction. The final DNA mixture containing both the blank and the enzyme associated labels with a 20% PhiX spike was sequenced with an Illumina MiSeq instrument and cartridge.

Partial cytochrome c oxidase purification from mitochondria

Frozen mitochondria were diluted with 10 mM Tris, pH 8.0 to give a 15 g/l protein concentration. This volume was used to calculate $(NH_4)_2SO_4$ additions. The suspension was solubilized by adding 0.6 g deoxycholate for each g of protein from a 10 w/v% stock solution. Proteins were first precipitated by adding 0.15 × volume saturated $(NH_4)_2SO_4$ solution. The precipitate was centrifuged down and the supernatant was transferred. To the supernatant another 0.1 × volume saturated $(NH_4)_2SO_4$ solution is added, mixed and centrifuged again. The resulting green pellet containing cytochrome c oxidase was dissolved, and solution was exchanged if needed with 10 mM Tris, pH 8.0, 25 w/v% glycerol, 0.1 w/v% deoxycholate and stored frozen.

4. Results

4.1 2-oxobutyrate interference with substrate-level phosphorylation

As a first step, we confirmed that externally added 2-oxobutyrate can enter through the mitochondrial inner membrane and undergo metabolism. This could be seen by the polarisation of liver and brain mitochondria upon addition of 2-oxobutyrate (Fig. 4, 5). The metabolism capacity was limited; subsequent additions did not yield a proportional increase in polarisation. Evidence for metabolism could also be observed in the minor increase in respiration (Fig. 6A).

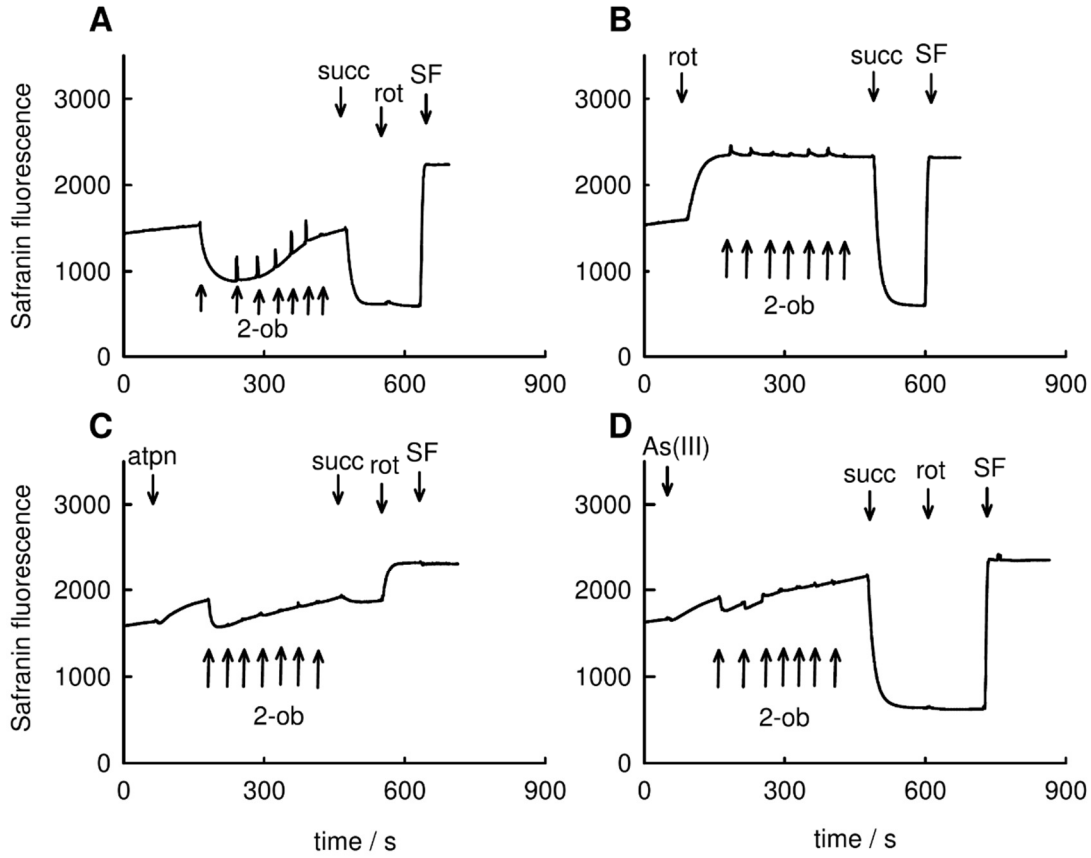

*Figure 4, The effect of sequential 0.5 mM 2-oxobutyrate (2-ob) additions on membrane potential (safranin fluorescence) with 0.5 mg liver mitochondria. (**A**) control and (**B**-**D**) inhibited conditions after endogenous metabolites were depleted in a 30-minute pre-incubation. 5 mM succinate (succ) and 250 nM SF-6847 (SF) were added afterwards to indicate functional integrity. Abbreviations: rot, 1 µM rotenone; atpn, 1 µM atpenin A5; As(III), 1 mM sodium arsenite. Source: Bui et al. (84) from repeated experiments.*

2-oxobutyrate uptake seemed to depend on an endogenous metabolite or the remaining membrane potential, because excessive pre-incubation time or prior ADP addition prevented any noticeable change in membrane potential. The metabolism-associated membrane polarisation was sensitive to rotenone and arsenite (membrane polarisation by complex I oxidation of NADH from the oxoacid dehydrogenase), as well as atpenin (membrane polarisation by downstream succinate oxidation) according to expectations.

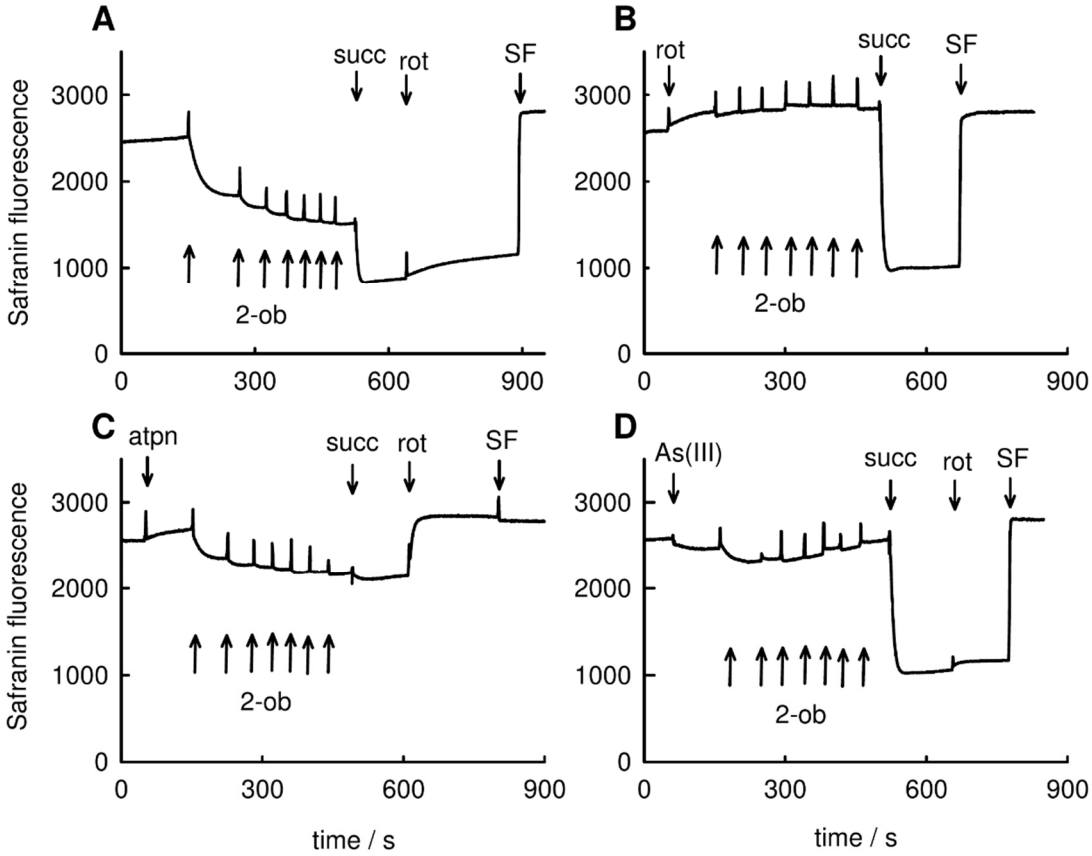

*Figure 5, The effect of sequential 0.5 mM 2-oxobutyrate (2-ob) additions on membrane potential (safranin fluorescence) with 0.5 mg brain mitochondria. (**A**) control and (**B**-**D**) inhibited conditions after endogenous metabolites were depleted in a 30-minute pre-incubation. 5 mM succinate (succ) and 250 nM SF-6847 (SF) were added afterwards to indicate functional integrity. Abbreviations: rot, 1 μM rotenone; atpn, 1 μM atpenin A5; As(III), 1 mM arsenite. Source: Bui et al. (84).*

Next, we used our already established method to interrogate, how various concentrations of 2-oxobutyrate influence substrate-level phosphorylation. By inhibiting complex I with rotenone, we create pseudoanoxic conditions mimicking the inhibition by the lack of oxidised electron carriers in the electron transport chain in the absence of the

terminal electron acceptor oxygen. The NAD/NADH ratio decreases, and without H^+ translocation by complex I and the downstream electron transport chain, the mitochondrial membrane potential (in absolute value) decreases below point of ATP synthase reversal.

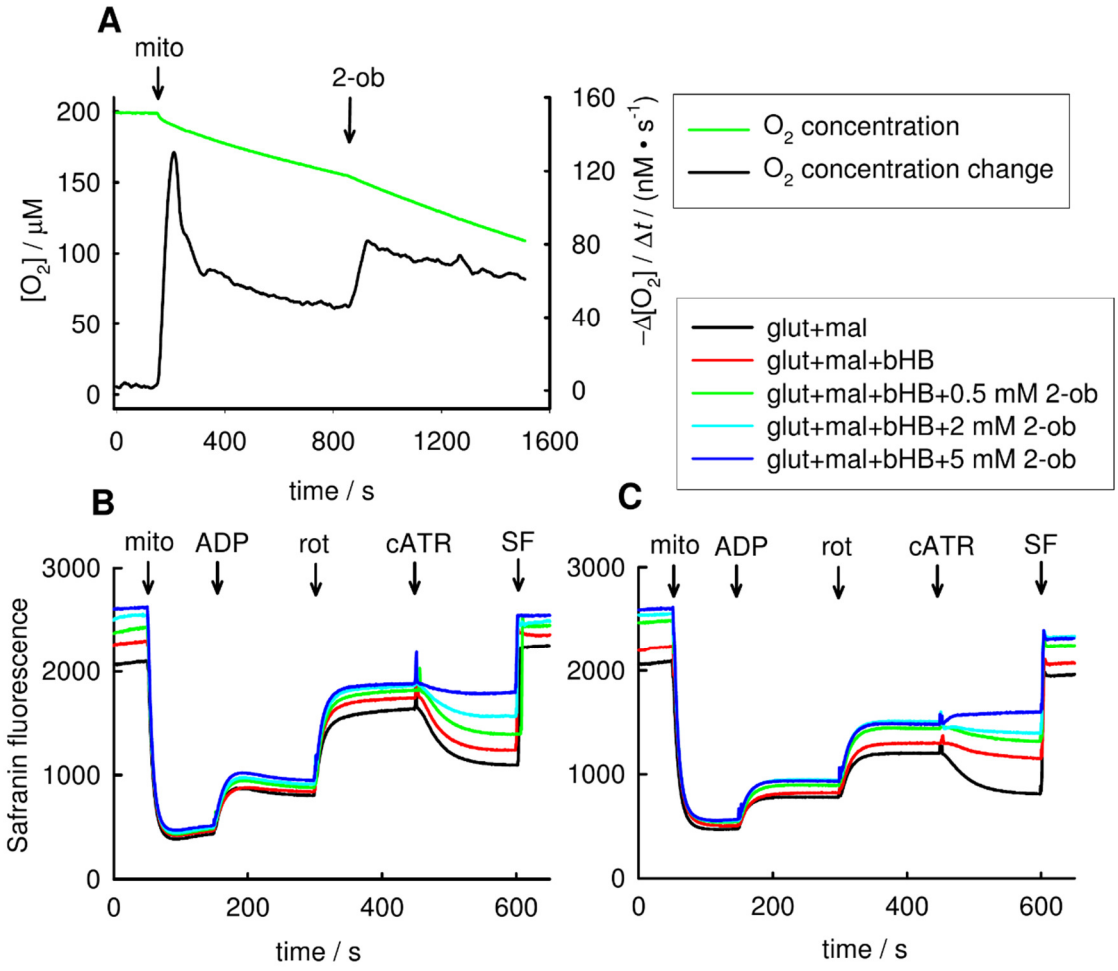

Figure 6, 5 mM 2-oxobutyrate (2-ob) addition increased respiration (-Δ[O₂]/Δt) with 1 mg liver mitochondria ***(A)****. Diminishing 1 µM carboxyatractyloside-induced (cATR) membrane polarisation (safranin fluorescence) change with 0.5 mg brain* ***(B)*** *or liver* ***(C)*** *mitochondria in the presence of increasing 2-oxobutyrate concentrations. Mitochondria were fueled with 5 mM glutamate (glut) and 5 mM malate (mal). 10 mM 3-hydroxybutyrate (bHB) was used to lower baseline substrate-level phosphorylation, the effective concentration was variable between days. Abbreviations: mito, mitochondria; rot, 1 µM rotenone; SF, 250 nM SF-6847; [O₂], oxygen concentration. Source: Bui et al. (84).*

This results in mitochondria becoming reliant on ATP hydrolysis by ATP synthase for membrane potential maintenance. The change in polarisation upon ANT inhibition with carboxyatractyloside (cATR) indicates the availability of ATP in the matrix from substrate-level phosphorylation. If STK provides enough ATP to prevent ANT reversal and ATP import, then ANT inhibition results in a polarisation increase. If there isn't enough ATP in the matrix and ANT is bringing external ATP in for hydrolysis, then the transport inhibition will result in a depolarisation. The combination of glutamate and malate supplies a strong STK mediated substrate-level phosphorylation. This is diminished by decreasing the NAD availability with 3-hydroxybutyrate through 3-hydroxybutyrate dehydrogenase. Increasing concentrations of added 2-oxobutyrate resulted in a trend of increasing depolarisation upon ANT inhibition with both liver and brain mitochondria (Fig. 6B, C). This means, the metabolism from increasing 2-oxobutyrate concentrations decreased the ATP availability and increasingly prevented ANT from operating in its forward (ATP export) direction.

4.2 Malate dehydrogenase for substrate-level NAD regeneration

We used our assay based on ANT inhibition to compare the ATP provision by STK under SDH inhibition in anoxia with both our standard glutamate plus malate combination and with 2-oxoglutarate plus aspartate. We have seen in the past that in anoxia, atpenin prevented substrate-level phosphorylation with glutamate and malate (Fig. 7D). By replacing malate with aspartate and glutamate with 2-oxoglutarate, we were able to rescue the pathway and prevent ANT reversal (Fig. 7A). If only glutamate was replaced with 2-oxoglutarate to reduce the number of NAD requiring steps, substrate-level phosphorylation could still not operate sufficiently (Fig. 7B). In comparison, even when the NADH burden was increased with glutamate, using the aspartate derived oxaloacetate, MDH2 was able to bring ANT to an approximately neutral state. Neither exporting nor importing ATP at a considerable rate (Fig. 7C).

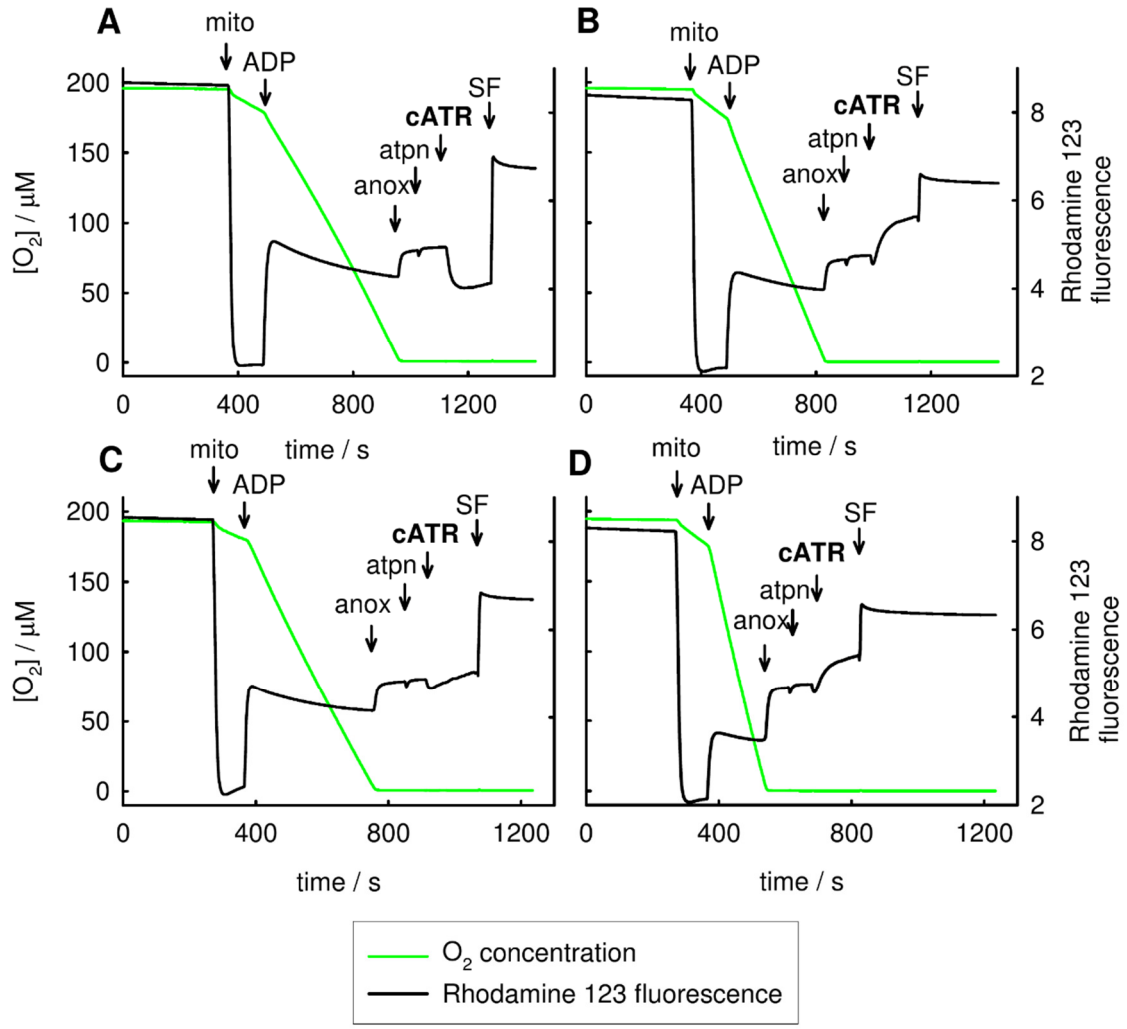

*Figure 7, Measuring the extent of substrate-level phosphorylation in anoxia under 1 µM atpenin (atpn) inhibition with the 1 µM carboxyatractyloside-induced (cATR) membrane polarisation (rhodamine 123 fluorescence) change in the presence of various respiratory substrate combinations. (**A**) 2-oxoglutarate + aspartate; (**B**) 2-oxoglutarate + malate; (**C**) glutamate + aspartate; (**D**) glutamate + malate. Each substrate was used at 5 mM concentration. 2 mM ADP-stimulated respiratory rate and steady-state membrane polarisation are dependent on the respiratory substrate. Abbreviations: mito, 1 mg mitochondria; anox, anoxia; SF, 250 nM SF-6847; [O_2], oxygen concentration. Y-axes are the same on all graphs.*

4.3 Succinate dehydrogenase reversal

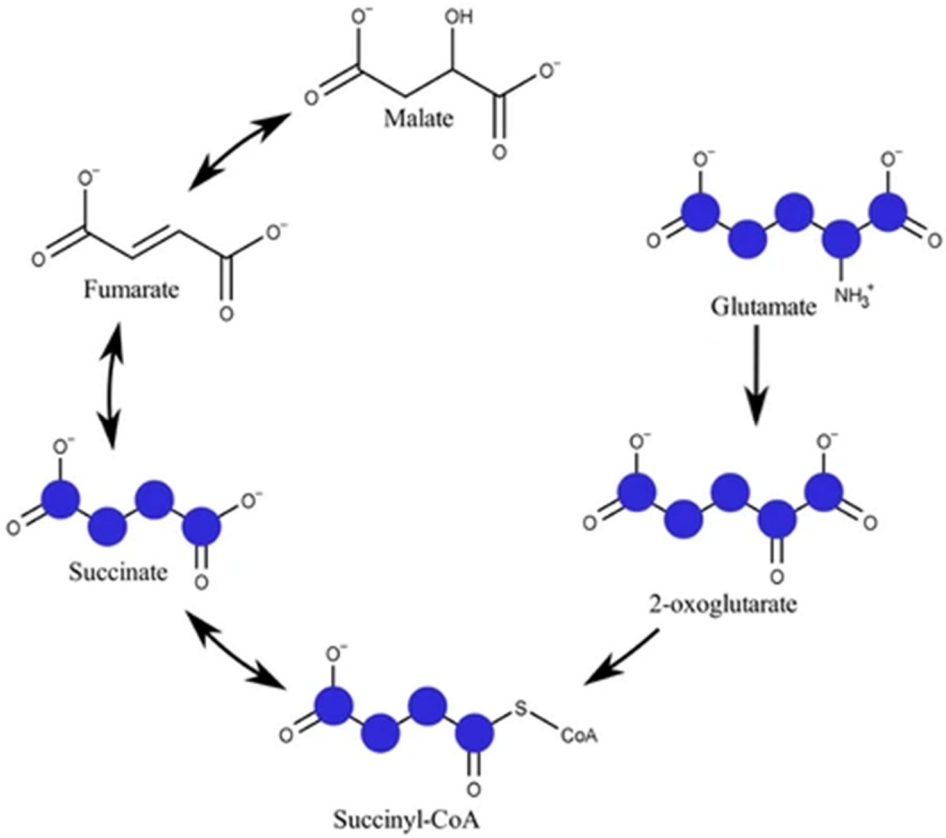

Figure 8, A scheme showing the metabolic conversion of glutamate-$^{13}C_5$ (M+5) into succinate-$^{13}C_4$ (M+4). Blue circles indicate the ^{13}C atoms. At the same time M+0 malate is converted to M+0 succinate (the latter is not shown). Source: Ravasz et al. (85) with slight modifications.

We tracked downstream metabolites from light malate (M+0) and mixed light/heavy glutamate (M+0/M+5) using mass spectrometry (Fig. 8). This replicates best the conditions used in previously established and published experiments. We can generally assume that different isotopologues of the same compound from a given sample ionize with the same relative efficiency during the injection into the mass spectrometer. However, without rigorous calibration and validation, the same is not true for two different metabolites due to unaccounted ion suppression effects. Therefore, we cannot directly compare the chromatographic peak areas of different compounds. Instead, we can express concentrations using the self-referential isotopologue distributions and the stoichiometric conversion. If we use two convergently metabolised substrates (glutamate and malate) and one of them is isotopically labelled, we can calculate the metabolic fluxes

towards their converging point (succinate) based on the absolute concentration change of that single metabolite and the isotopologue ratios in the adjacent steps (KGDHC and SDH). Results of the metabolite quantification are shown in Tabl. 1.

Table 1, The average measured norleucine-normalised succinate concentrations, isotopologue distributions and their respective standard deviations that was used to calculate the flux contributions from malate and glutamate (n = 6 from 2 replicates with 3 samples each). Both the light M+0 and heavy M+4, M+5 isotopologues are shown for every experiments. Data source: Ravasz et al. (85).

	Succinate amount		Succinate % distribution		Fumarate % distribution		2-oxoglutarate % distribution	
	M+0	M+4	M+0	M+4	M+0	M+4	M+0	M+5
0 s	61.8 ± 6.3	1.8 ± 0.3	97.0 ± 0.3	2.8 ± 0.3	98.64 ± 0.27	0.25 ± 0.05	77.0 ± 0.7	22.9 ± 0.7
200 s	65.1 ± 4.2	3.8 ± 0.3	94.0 ± 0.3	5.5 ± 0.2	99.16 ± 0.31	0.29 ± 0.02	62.0 ± 0.4	37.7 ± 0.4
600 s	79.7 ± 5.1	6.0 ± 0.9	92.4 ± 0.9	6.9 ± 0.8	99.08 ± 0.17	0.34 ± 0.04	54.3 ± 1.1	45.3 ± 1.1
600 s with atpenin	59.7 ± 3.3	4.0 ± 0.4	93.2 ± 0.4	6.3 ± 0.3	98.98 ± 0.31	0.27 ± 0.04	55.3 ± 1.3	44.3 ± 1.4

The model in Fig. 9 was used to calculate the relative contributions of KGDHC and reverse SDH to succinate formation.

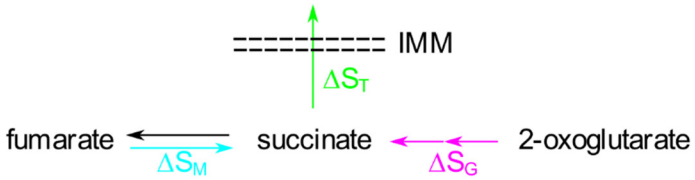

Figure 9, The model that was used for calculating metabolic fluxes. ΔS_T is the amount of succinate transport through the inner mitochondrial membrane (IMM). ΔS_M is the amount of malate conversion to succinate or vice versa. ΔS_G is the amount of glutamate conversion to succinate. Source: Ravasz et al. (85).

From the model in Fig. 9 the following equations can be written on the basis of mass balance.

$$\Delta succinate^{(M+4)} = \Delta S_G \cdot R_{og}^{(M+5)} - \Delta S_T \cdot R_{succ}^{(M+4)} + \Delta S_M \cdot R_{fum}^{(M+4)}$$

$$\Delta succinate^{(M+0)} = \Delta S_G \cdot R_{og}^{(M+0)} - \Delta S_T \cdot R_{succ}^{(M+0)} + \Delta S_M \cdot R_{fum}^{(M+0)}$$

Where ΔS_G, ΔS_M, ΔS_T are the unknown metabolic fluxes from the direction of glutamate, malate and transport respectively. R_{og}, R_{succ}, R_{fum} are the ratios of the superscripted isotopologue of 2-oxoglutarate, succinate and fumarate respectively. We first checked the operating direction of succinate dehydrogenase, by taking $R_{fum}^{(M+4)}$ as practically zero. This is a good initial approximation considering $R_{fum}^{(M+4)}$ was in all cases less than 0.5% (Tabl. 1). This means all labelled succinate originates from 2-oxoglutarate. The unaccounted change in $\Delta succinate^{(M+0)}$ will indicate whether fumarate was being reduced and thus ΔS_M is positive, or succinate was being oxidised and thus ΔS_M is negative. Oxidation by KGDHC is strictly unidirectional. ΔS_T was estimated based on the experiment with atpenin inhibition (fourth row in Tabl. 1), which renders the ΔS_M practically zero and simplifies the linear equations to two unknowns ΔS_G and ΔS_T. We assumed that ΔS_T is the same even without atpenin inhibition and constant over time. This seemed to be a reasonable approximation, since succinate concentrations (the driving forces) are very similar in all cases (Tabl. 1). If ΔS_T is calculated as a linear function of succinate concentration, the results change only very slightly. We assumed that succinate transport was unidirectional. We did not add any exogenous succinate and therefore the higher succinate concentration inside mitochondria should drive the transport outwards. We did not see significant amounts of partially labelled (i.e. M+1, M+2, M+3) metabolites, therefore only the isotopically homogenous metabolites are taken into consideration in our model. The experimental difficulty came from preserving the momentary state at sampling. We noticed artefacts from aerobic metabolism occurring during sample collection in previous experiments. To best reflect the intramitochondrial conditions, we avoided the most common quick denaturation techniques (such as strong acids or detergents), which would result in the averaging and dilution with the extramitochondrial medium. Instead, we used an inhibitor mixture that would prevent further interconversion and transport. Among others, cyanide was added to prevent potential aerobic artefacts. We expected a more rapid equilibration after the heavy

glutamate addition, but the isotopologue ratios were noticeably gradual at subsequent time points (Fig. 10). To account for the time dependence, we fit an exponential model to the few points we had and used the area under the curve to calculate a representative average for each required time interval.

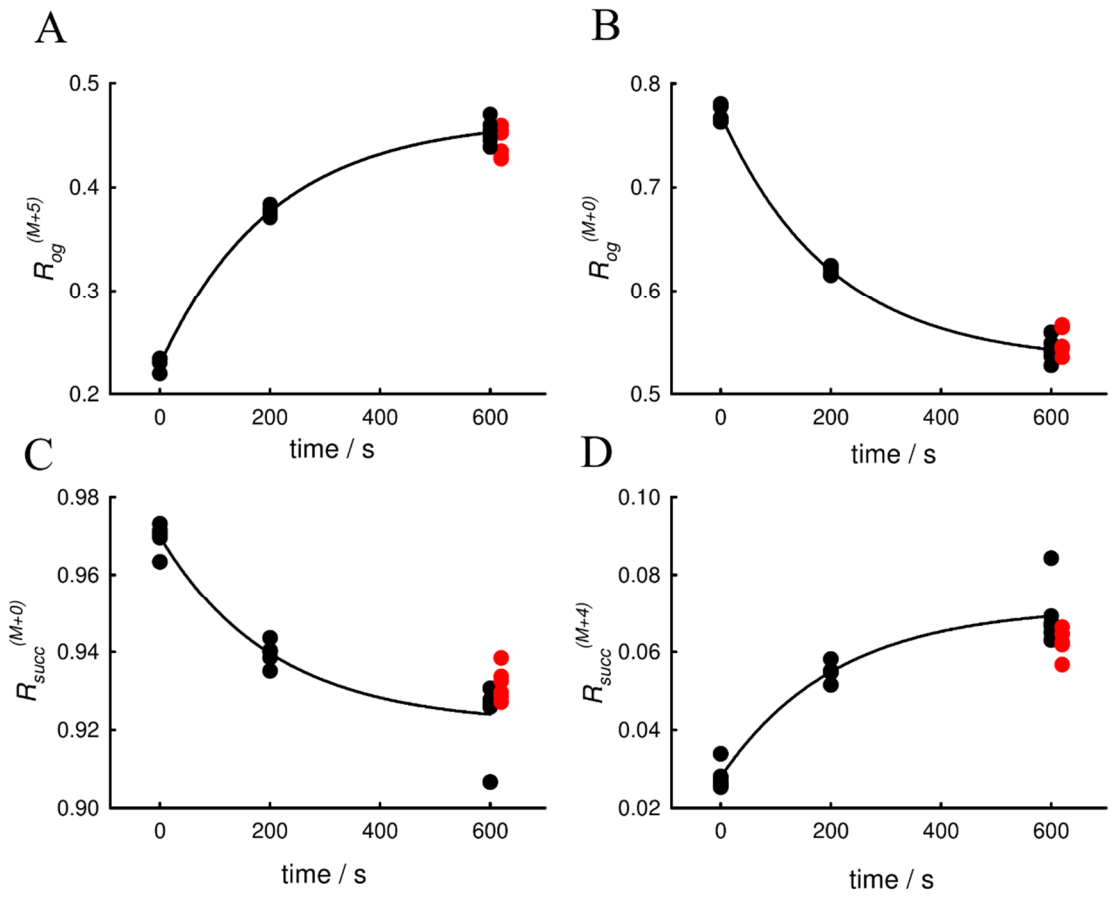

Figure 10, The change in isotopologue ratios over time. $R_{succ}^{(M+0)}$, $R_{succ}^{(M+4)}$, $R_{og}^{(M+0)}$, $R_{og}^{(M+5)}$ *representing M+0 succinate, M+4 succinate, M+0 2-oxoglutarate, M+5 2-oxoglutarate respectively. Fumarate isotopologue distributions did not noticeably change. The continuous lines represent the exponential fits. Black dots are the standard glutamate-malate experiments; red dots are the experiments with added atpenin. Red dots are slightly offset to the side to avoid cluttering. Source: Ravasz et al. (85), supplementary materials with slight modifications.*

Calculated results in Tabl. 2, show that as more time elapses in anoxia, the contribution from SDH increases and overtakes KGDHC. Meaning, NADH oxidation is offset to a significant degree by the reverse operation of SDH. Numerically, we calculated SDH turnover to be approximately 2.78 times more than KGDHC. This is slightly more than

the stoichiometry of 2 (1 electron pair from glutamate dehydrogenase and 1 electron pair from KGDHC) that would be required to offset the electrons for substrate-level phosphorylation.

Table 2, Comparative metabolite fluxes through the opposing pathways in the acute (0-200 s) and sustained (200-600 s) phases of anoxia with their respective standard error (n = 6 from 2 replicates with 3 samples each). Errors were calculated using Gauss' law of error propagation with linear approximation from the constituent errors. Data source: Ravasz et al. (85).

	0-200 s average	200-600 s average
succinate from glutamate	3.4 ± 0.3 s^{-1}	1.4 ± 0.2 s^{-1}
succinate from malate	0.4 ± 1.7 s^{-1}	3.9 ± 0.9 s^{-1}
succinate export	1.1 ± 0.6 s^{-1}	1.1 ± 0.6 s^{-1}

4.5 Safranin as a potential electron acceptor

We began the project with cyclic voltammetry, on one hand, to see the polarisation required for detection with our electrodes, and on the other hand, to see if there were any other interfering signals. The cathodic peak was around -585 mV and the anodic peak was around -515 mV with a 50 mV/s scanning rate. We could also observe the following: safranin was highly adsorptive, the peak potentials were dependent on safranin's concentration and the scanning rate, the electrode reaction was not reversible (in other words, an overpotential was required), and no other peaks were detected. Based on this information, we used a working electrode polarisation of -100 mV or higher for reduced safranin detection. More negative potentials would only increase the interference from oxygen while it is present. We used various respiratory substrates to screen for any possible artificial reduction. Ubiquinone-2 was also added initially as a positive internal control. While oxygen was present, we did not see anything unexpected, but when mitochondria got to anoxia without malate, we saw a continuous increase in reduced mediators, implying the reduction of safranin (Fig. 11A, B). We also saw the fluorescence starting to decrease after prolonged anoxic exposure, which was another indicator for the reduction, since reduced safranin is colourless *(*Fig. 11D*)*.

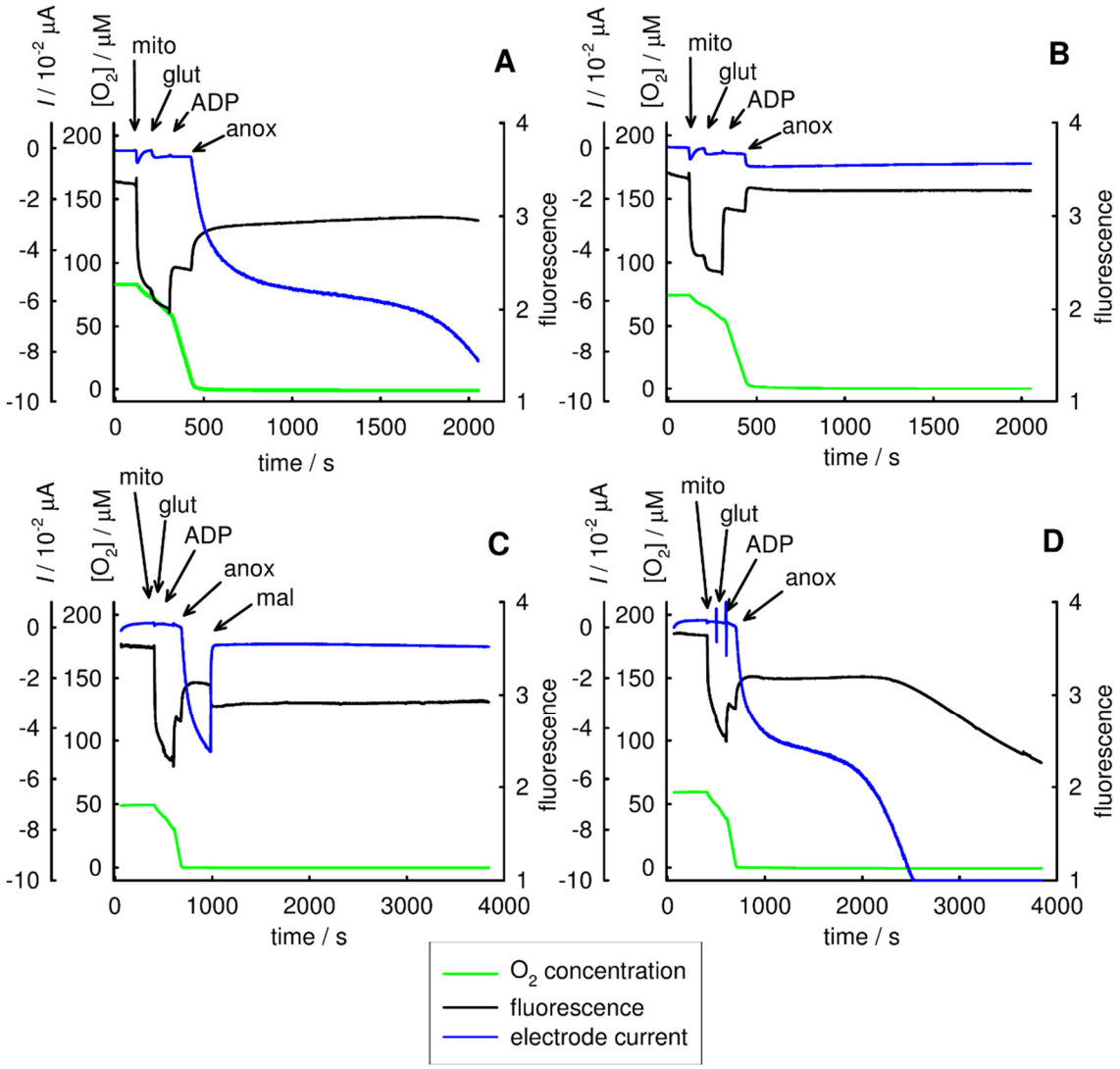

Figure 11, Recordings with 1 mg liver mitochondria showing the simultaneously measured electrode current (I), oxygen concentration ([O_2]) and fluorescence. Reduced species formation in anoxia was observed with safranin ***(A)****, but not with control rhodamine 123* ***(B)****. Both contained 1 µM ubiquinone-2 positive control.* ***(C)*** *shows the absence of change in the presence of malate.* ***(D)*** *shows the fluorescence changing after prolonged anoxia along with the increasing current. Initial solutions were partially purged with argon gas to reduce the initial dissolved oxygen concentration and speed up experiments. 2 mM ADP was added at the indicated time. Abbreviations: mito, mitochondria; glut, 5 mM glutamate; anox, anoxia; mal, 5 mM malate.*

Next, we investigated, why we did not see anything when malate was present (Fig. 11C). When we inhibited SDH with atpenin, we could detect the restored safranin reduction amperometrically. However, we did not see any decreasing fluorescence (Fig.

12). Using either fumarate or malate, with different SDH inhibitors (atpenin, malonate, carboxin, thenoyltrifluoroacetone), gave the same results. Based on these experiments, it seems that SDH either mediates the oxidation of reduced safranin or prevents the safranin reduction from occurring. The most interesting results were with succinate, because it was not only capable of stopping SDH reversal and therefore making reduced safranin detectable with the electrode, but also prevented the reduction associated fluorescence decrease, even in the absence of malate. Notably, in cases when we did not see a fluorescence decrease, but measured an increase in current, the current tended to remain in a moderate domain. Meaning, the reduced safranin concentration did not increase further beyond a point.

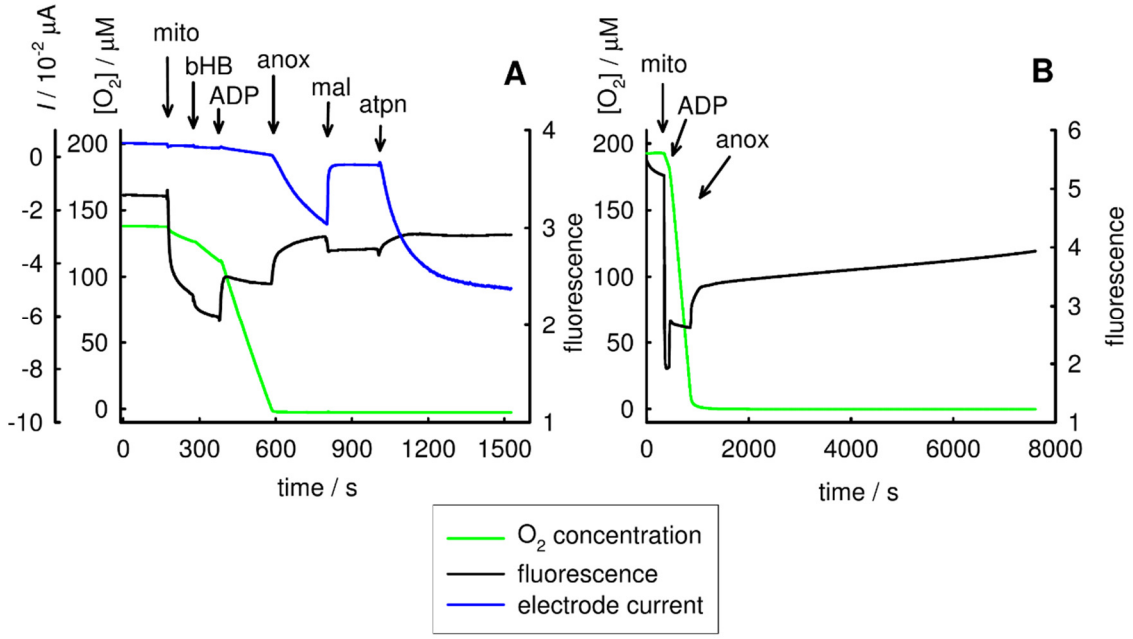

Figure 12, The conflicting manifestation of reverse SDH inhibition. ***(A)*** *Electrochemical detection showed immediate current (I) increase after SDH inhibition with 1 µM atpenin (atpn),* ***(B)*** *no decrease in safranin fluorescence after prolonged anoxia. (B) already contained 5 mM 3-hydroxybutyrate (bHB), 5 mM malate (mal) and 1 µM atpenin before the start of the experiment. 2mM ADP was added at the indicated time. (A) was partially purged with argon. Abbreviations: mito, 1 mg mitochondria; anox, anoxia; [O₂], oxygen concentration.*

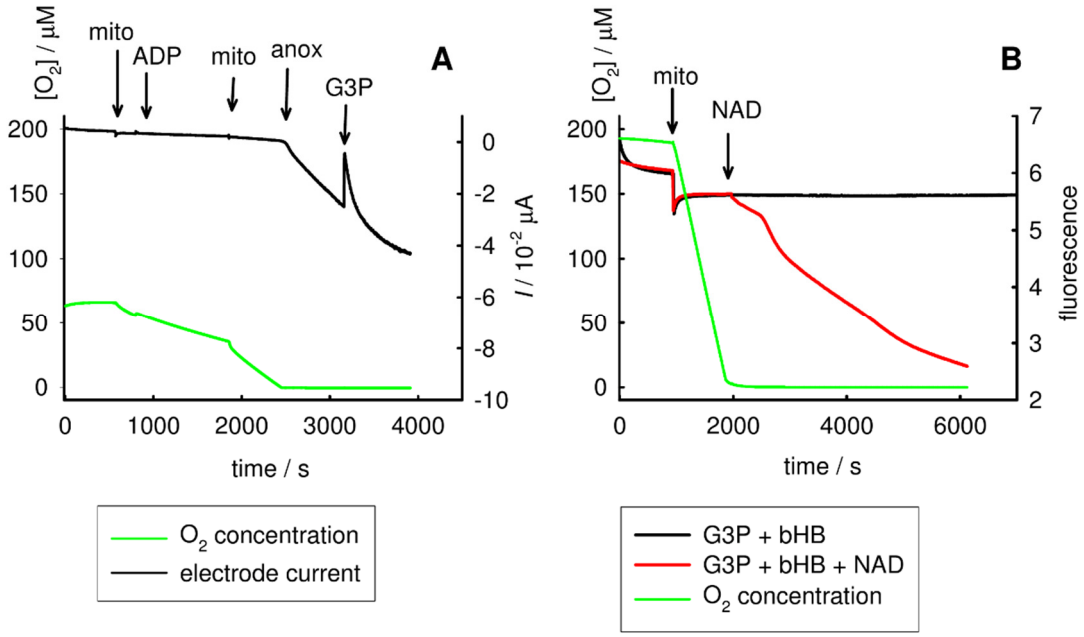

Figure 13, ***(A)*** *Safranin-associated current (I) in anoxia with 2x1 mg liver mitochondria (mito) without any added substrate initially. 2 mM ADP was added at the indicated time.* ***(B)*** *Safranin fluorescence change with 1 mg mitochondria permeabilized by freezing. Oxygen curve is from only one of the experiments in the case of (B) for illustration to avoid cluttering. 0.5 mM NAD was added at the indicated time. (A) was partially purged with argon before the experiment. Abbreviations: G3P, 10 mM sn-glycerol-3-phosphate; bHB, 5 mM 3-hydroxybutyrate; [O2], oxygen concentration.*

We looked for the possible source of electrons. Intact mitochondria seemed to be indifferent to the nature of respiratory substrates. Even without any exogenous respiratory substrates the initial reduction was observable amperometrically (Fig. 13A) and sn-glycerol-3-phosphate by itself was also sufficient for fluorescence decrease. On the other hand, permeabilized mitochondria showed a strong requirement for NADH or NAD plus an associated substrate (Fig. 13B), but was unaffected by the direct ubiquinone substrate sn-glycerol-3-phosphate. Using NADH with a partially purified cytochrome c oxidase preparation, which also contained atpenin sensitive SDH along with cytochrome c oxidase, only fumarate had an oxidative effect and was partially mitigatable with malonate (Fig. 14B). Malate was no longer capable of producing the same result. Comparatively, if whole mitochondria were used in the presence of detergent, malate behaved similarly to fumarate (Fig. 14A).

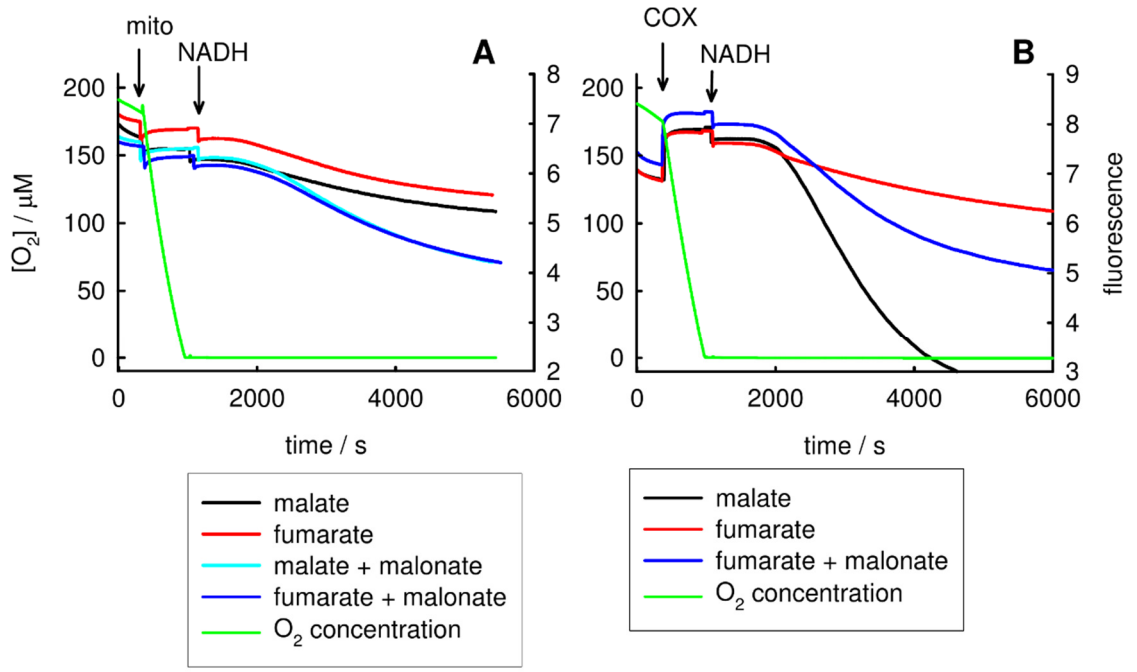

Figure 14, The change in safranin fluorescence with ***(A)*** *1 mg frozen liver mitochondria* ***(B)*** *crude SDH and cytochrome c oxidase preparation. Both solubilized with 0.1 w/v% triton X-100 and the indicated substrates were added at 2.5 mM concentration or malonate at 5 mM. Oxygen was depleted using 0.01 w/v% ascorbic acid, 50 µM tetramethylphenylenediamine, 10 mg/l cytochrome c as cytochrome c oxidase substrates. 0.5 mM NADH was added when indicated after anoxia was reached. Oxygen curve is from one respective experiment for illustration to avoid cluttering. Abbreviations: mito, mitochondria; COX, cytochrome c oxidase preparation.*

The difference between the two results was likely caused by the absence of fumarase in the partially purified enzyme preparation. If atpenin was used instead of malonate, the change in safranin fluorescence was seemingly exactly the opposite. Atpenin decreased safranin reduction with solubilized mitochondria. This implies that the flavin site of SDH may play a direct role, but the quinone site does not. Since fluorescence still decreased over time even in the presence of malate or fumarate, we can conclude that reduced safranin oxidation by SDH has only a limited capacity. Under the above mentioned conditions safranin reduction eclipsed this capacity.

We made experiments to address whether the reaction was mediated by an enzyme at all, or whether it was a chemical reaction without enzymatic catalysis. We noticed that

the continuous light excitation of safranin in the presence of NADH caused an increase in oxygen consumption proportional to the light intensity (Fig. 15A).

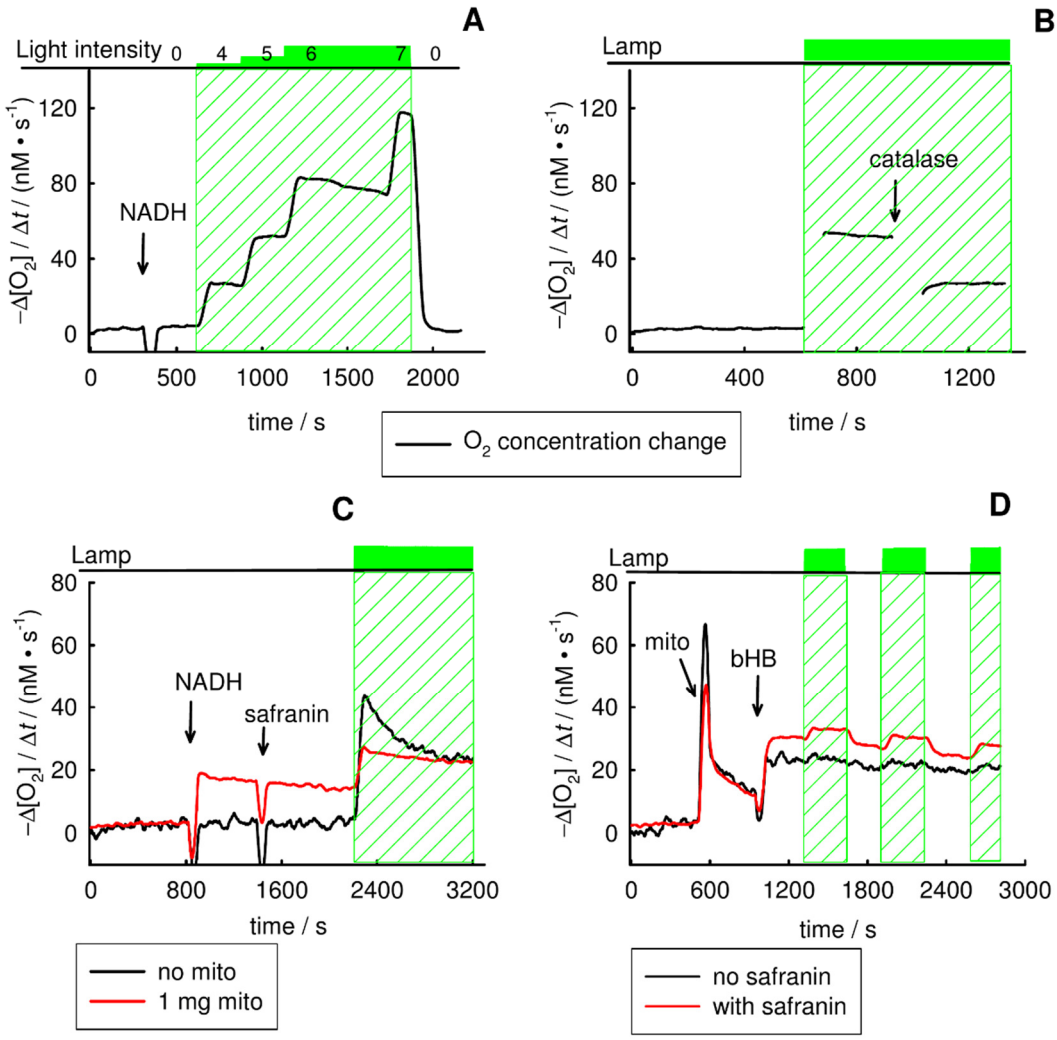

Figure 15, Oxygen consumption rate -Δ[O₂]/Δt under various conditions. ***(A)*** *light intensity dependent oxygen reduction with 0.5 mM NADH and safranin.* ***(B)*** *oxygen consumption with NADH and safranin getting halved by catalase.* ***(C)*** *light sensitive oxygen reduction with 1 mg permeabilized mitochondria.* ***(D)*** *light sensitive oxygen reduction with 5 mM 3-hydroxybutyrate (bHB) fueled 1 mg intact mitochondria (mito) under 1 mM cyanide inhibition. Illuminated segments are indicated with green diagonal stripes.*

The oxygen consumption was approximately halved upon 500 U of catalase addition (Fig 15B), indicating oxygen reduction to hydrogen-peroxide. All three components: light, NADH, safranin were necessary. If any of them was missing, there was no oxygen reduction to hydrogen peroxide (Fig. 16B). We used the hydrogen peroxide generation to

check excitation-wavelength-dependence. We found that the amount of hydrogen peroxide formed at a given wavelength correlated well with safranin's absorption spectrum, but remained near background at lower wavelengths, where NADH absorbs (Fig. 16A). There was a significant background due to hydrogen peroxide formation with just NADH and horseradish peroxidase (86), therefore it was necessary to degrade the excess NADH after light exposure under acidic conditions (87). The degradation was almost complete, and most of the NADH interference could be eliminated by this. The remaining acid insensitive background was stable across samples, giving an approximate absorbance of 0.1.

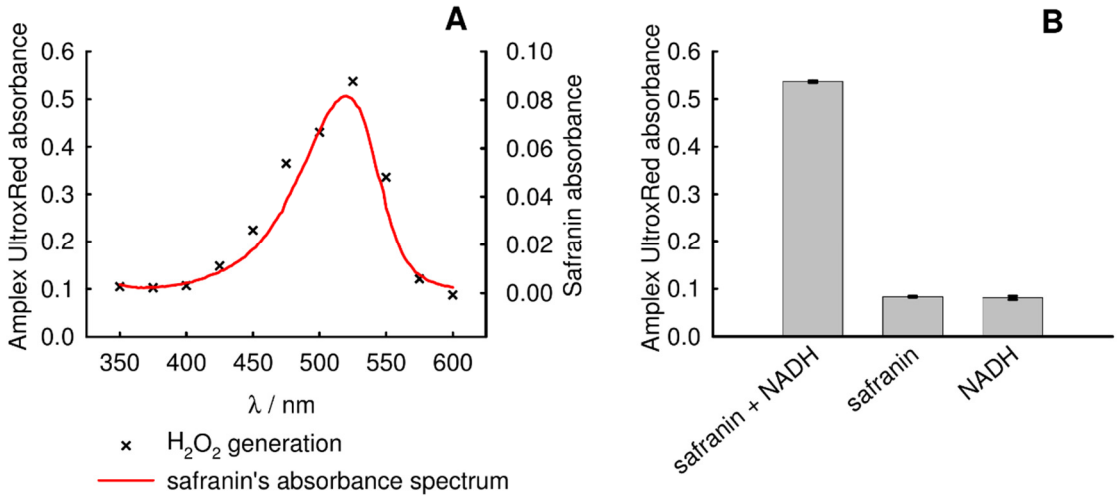

Figure 16, ***(A)*** *The amount of H_2O_2 generated (Amplex UltroxRed absorbance) by the safranin–NADH reaction measured at 25 nm increments overlapped in the wavelength domain with safranin's absorption spectrum.* ***(B)*** *The amount of hydrogen peroxide generated (Amplex UltroxRed absorbance) with 525 nm light excitation, with or without NADH and safranin (n = 3). For (B) error bars represent standard error.*

We examined whether there was a distinguishable mitochondrial contribution in addition to the non-enzymatic reaction. When we used permeabilized mitochondria, we saw that there was no observable reaction without light, and the light-dependent oxygen consumption was less (Fig. 15C). Presumably, the latter was caused by the increased light scattering or increased light absorption, leaving less photons for the photoinduced reaction. When we repeated previous experiments in parallel with and without continuous light excitation, we noticed a large discrepancy in the fluorescence decrease (Fig. 17B). In fact, in the absence of illumination there was very little, if any safranin reduction. Furthermore, we made similar experiments with intact mitochondria. This time, we saw

only a very minor increase in oxygen consumption under cytochrome c oxidase inhibited conditions upon turning the light on (Fig. 15D). However, even without light, intact mitochondria did seemingly reduce safranin to some extent (Fig. 17A). This could be potentially enzyme-mediated.

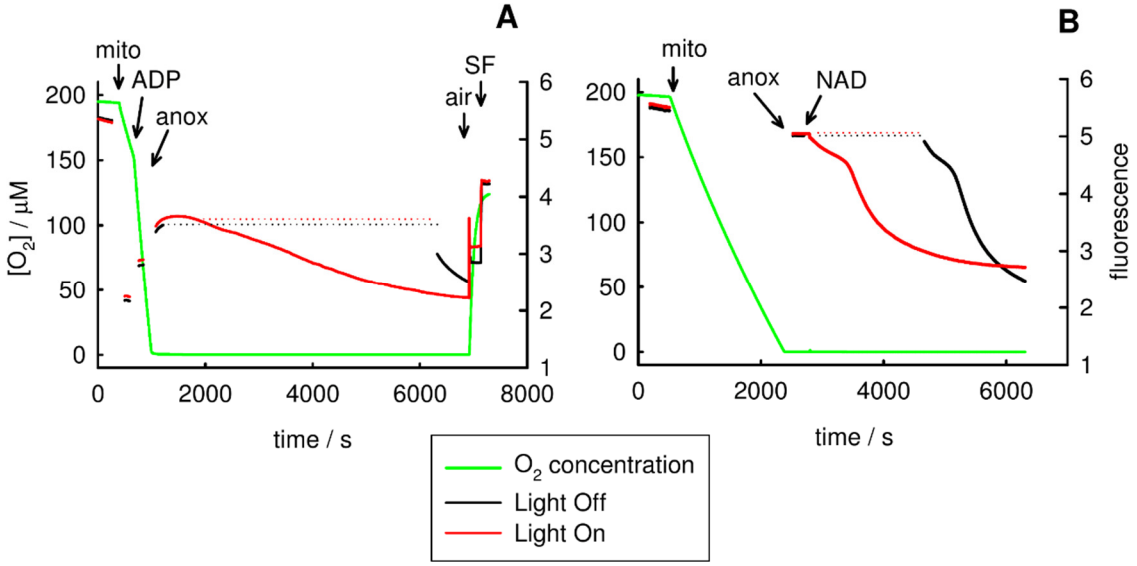

Figure 17, Safranin fluorescence measurements with ***(A)*** *1 mg intact mitochondria (mito),* ***(B)*** *1 mg permeabilized mitochondria with and without continuous illumination in anoxia. The dotted horizontal lines extend the respective measured fluorescence values, from when one of the lights was turned off, until it was turned back on again, for comparison. Oxygen concentration [O_2] curve is from one of the respective experiments only for illustration to avoid cluttering. In both experiments, mitochondria was fueled by 5 mM 3-hydroxybutyrate and 5 mM sn-glycerol-3-phosphate. 2 mM ADP and 0.5 mM NAD was added when indicated. Re-aeration and 250 nM SF-6847 (SF) was added to check mitochondrial integrity. The axes are the same for both graphs.*

4.6 Expressing and screening STK

As it was mentioned in the objectives, to be able to do all the experiments necessary to find an inhibitor for STK, we first need to possess the purified target enzyme. Sherley et al. have already successfully expressed the recombinant enzyme, so we used the information they previously published (88). For recombinant expression, the coding region used the co-expression structure of pETDuet-1 and the coding sequences were inserted after the two ribosome binding sites with only one transcription terminator at the very end. This region was then inserted into a pET-42a vector plasmid. Expression with

transformed BL21(DE3) Escherichia coli was controlled by lac operons and kanamycin resistance was used for selection. We attached two different affinity tags to the two subunits for easier downstream purification. From published structures of related proteins found in the Protein Data Bank, we knew the two C-terminals were both sufficiently flexible and exposed to accommodate the tags. The N-terminal sequence of the beta subunit was modified according to the work done previously by others to Met-Ser-Leu (88). At first, the purification was done with two subsequent affinity column steps. In our case, 100 mM imidazole was sufficient for elution with a 6 amino acid long His-tag. Metal affinity chromatography was put as the first step to remove the majority of contaminant proteins (Fig. 18/2,3). For the Strep-tag, we simply followed manufacturer specifications. This produced a preparation with most of the low molecular weight contaminants and monomeric alpha subunits removed (Fig. 18/5). While initial results were acceptable and the preparation was mostly made of STK's two subunits (33.5 kDa and 45.5 kDa), some higher molecular weight contaminants persisted (not visible on the photograph). We wanted to remove more of those contaminants to improve the quality further without too much loss. Using anion-exchange chromatography in negative mode (when the protein of interest is not retained) removed not only the monomeric alpha subunits, but also some persistent higher molecular weight contaminants and was therefore included in the standard purification procedure (Fig. 18/6,7). At a higher pH, when the protein bound to the anion-exchanger, the washing step was continuously removing the subunit with the higher isoelectric point, therefore we decided to use the exchanger in negative mode. Resolution is limited with gravity columns and there is likely a significant loss, but the improvement was noticeable, and the yield was still acceptable (approx. 1 mg protein per 2.8 g wet bacterial pellet). Based on the stability properties, some further minor adjustments were made to the purification procedure. For example, we incubated the enzyme with ATP and magnesium between two chromatography steps to ensure complete phosphorylation. Phosphorylating the protein improved stability and limited the possibility of both the phosphorylated and dephosphorylated form being present during the library screening. The resulting purity was around 98-99% based on the visual assessment on SDS-PAGE, with both subunits present at their respective mass range in approximately equal proportions (Fig. 18/8-10).

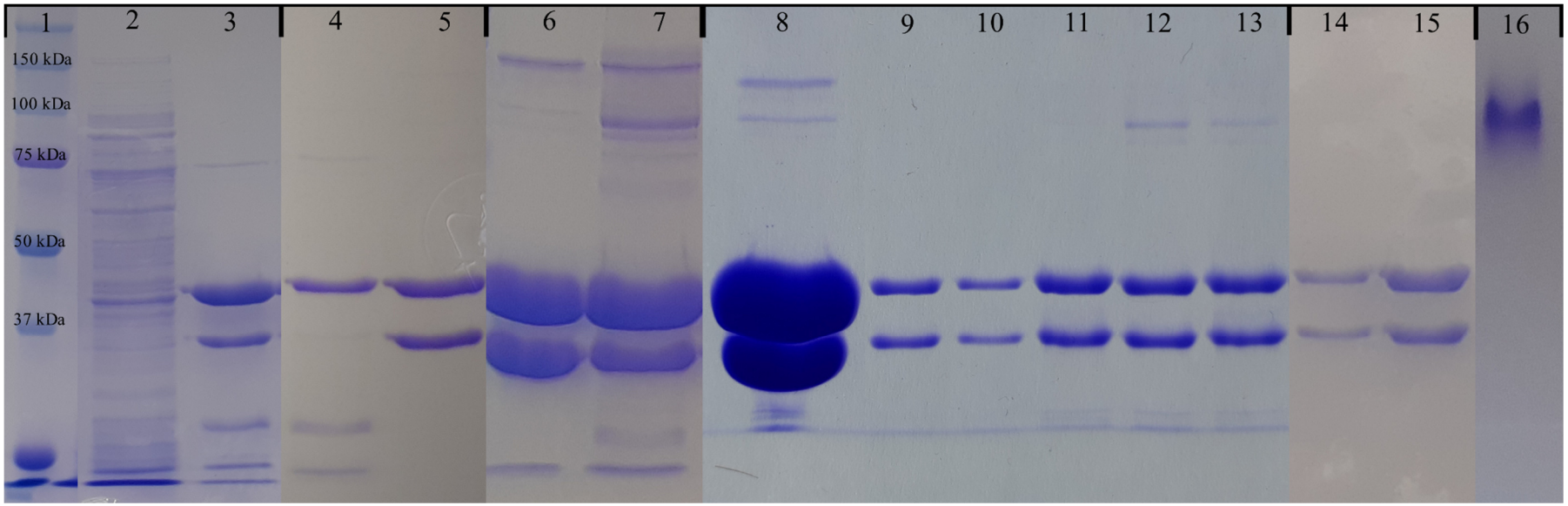

Figure 18, Polyacrylamide gel results. Only one Mw standard is provided, because the two subunits of STK function as secondary standards and the exact molecular weight is not the focus of the discussion. 1, Mw ladder standard; 2, Metal affinity chromatography wash; 3, Metal affinity chromatography elution; 4, Streptavidin affinity chromatography wash; 5, Streptavidin affinity chromatography elution; 6, Anion-exchange chromatography flow-through; 7, Anion-exchange chromatography elution; 8, concentrated final product; 9, 50-times diluted final product; 10, 100-times diluted final product; 11, initial sample for stability; 12, stability sample after 5 days of storage at 25°C; 13, stability sample after storage for 5 days at 25°C at a 10-times diluted concentration ; 14, surplus enzyme remaining unbound to magnetic beads; 15, enzyme eluted from magnetic beads; 16, STK preparation ran in a native PAGE. Black lines on the top indicate separate gels.

Native PAGE did not reveal the presence of noticeable amounts of aggregates (Fig. 18/16), but the slight light scattering at 330 nm could have been from a very small amount of aggregates.

While measuring activity, succinyl-CoA formation was not linear in the initial phase at lower enzyme concentration. The kinetic curve had an inflection point, where the rate (first derivative with respect to time) reached a maximum and decreased afterwards (Fig. 19A). At higher enzyme concentrations only the decreasing phase was observed. Adding small amounts of products did not change this observation. However, when we used the maximum velocities at the inflection points, they were linearly proportional to enzyme concentration (even if not crossing the origin), and therefore we used them to represent the enzyme's activity (Fig 19B).

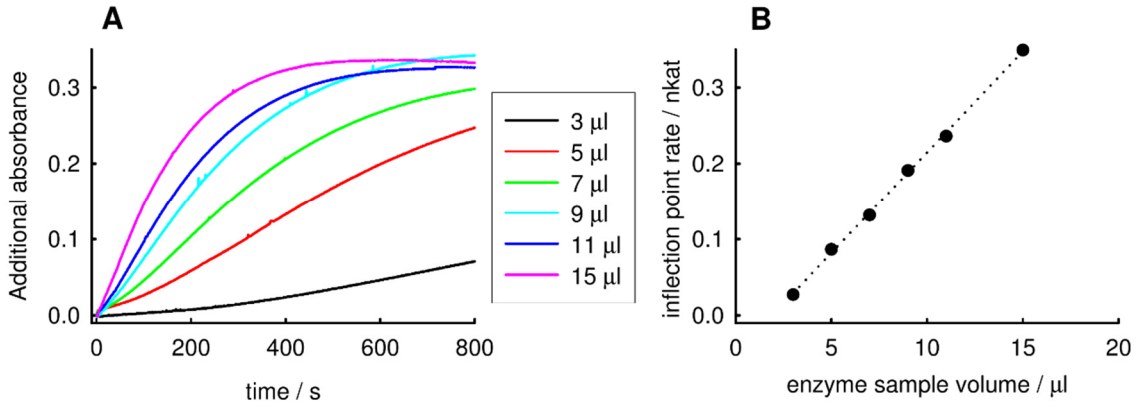

Figure 19, ***(A)*** *STK kinetic curves with incremental amounts of enzyme, measuring succinyl-CoA formation at 235 nm. The background absorbance from the substrates (0.95-1) was subtracted.* ***(B)*** *Plot of the measured maximum catalytic rates with respect to enzyme amount and a fitted linear model (dotted line).*

In order to ensure that our enzyme remained in the most native state possible until screening after purification, we made some stability experiments. These were based only on the retention of enzymatic functionality as the indicator of native state, without detailed structural analysis. Using HEPES as the buffering agent regardless of pH was highly unfavourable for stability and resulted in significant (>30%) activity loss even after just 1 day. Tris was found to be a far better buffering agent in terms of stability, even if the buffering capacity at neutral pH is comparatively lower (see Tabl. 3 absolute stability after 15 days). We tried various excipients to mitigate different kinds of denaturation (detergent, ionic strength, reductive buffer, etc.), but found none to be advantageous, except for phosphorylating conditions (ATP plus Mg^{2+}). SDS-PAGE showed some

indication of irreversible aggregate formation by bands appearing in the higher molecular weight region, but the extent of denaturation measured by activity loss did not correlate well with it (Fig. 18/11-13). Storing the enzyme less concentrated was preferable for stability. If the enzyme is stored for only a few weeks in the cold without freezing, the lowest possible glycerol concentration and a pH of 7.0-7.3 is recommended. If the enzyme is stored frozen for a long time, then a higher glycerol content and a pH of 7.6 can mitigate against the damage from freezing (Tabl. 3).

Table 3, STK storage stability in 50 mM pH 7-8 Tris buffer with 0-20% glycerol. Relative stability is expressed compared to the average of all the sample measurements; absolute stability is expressed compared to the initial day-zero reference measurement.

15 days 4°C				15 days frozen			
pH	Glycerol w/v%	Relative stability %	Absolute stability %	pH	Glycerol w/v%	Relative stability %	Absolute stability %
7	20	100.0	91.0	7	20	117.4	76.5
7.006	10	106.0	96.6	7.006	10	101.5	66.1
7.062	0	125.7	114.5	7.062	0	72.5	47.3
7.119	20	91.1	82.9	7.119	20	116.5	75.9
7.184	10	106.8	97.3	7.184	10	103.4	67.4
7.247	0	125.9	114.7	7.247	0	65.1	42.4
7.566	20	47.8	43.5	7.566	20	123.5	80.5
7.602	10	93.4	85.1	7.602	10	114.6	74.7
7.642	0	115.2	104.9	7.642	0	73.7	48.0
7.848	20	88.1	80.2	7.848	20	111.8	72.9

The rate of freezing (snap freezing with liquid nitrogen or slow natural freezing) did not have an impact on the retention of enzyme activity, neither did the subsequent storage temperature. Repeated freezing only came with minor additional denaturation. Generally, there is a significant ~20% initial loss upon freezing, but for storage over a very long time it becomes the preferable option.

Mass spectrometric measurements indicated that both polypeptide chains were missing the N-terminal initiator methionine and that the alpha subunit histidine was homogenously present in the phosphorylated form.

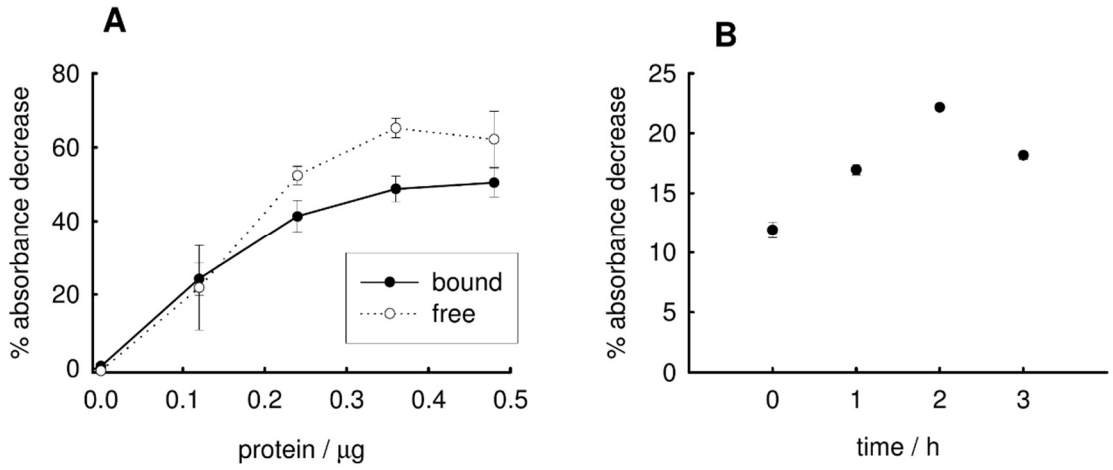

Figure 20, ***(A)*** *Bead-bound and free enzyme activity. Measured with the decrease in DTNB absorbance from free CoA sequestration. The amount of bound protein is only an estimated value calculated from previous binding experiments.* ***(B)*** *Short-term stability at room temperature with 0.4 µg bead-bound protein. The absorbance-decrease values in (B) are likely lower because of phosphate (product inhibition) carryover from the screening solution. Error bars represent standard deviation (n = 2).*

In preparation for the library screening, we assessed the protein-magnetic bead binding stoichiometry, as well as the stability of the enzyme bound to the bead over the duration of the expected incubation. We found that the binding site occupancy was proportional to the protein concentration used, and even at excess concentrations with unbound protein, further increasing the concentration increased both bound and unbound protein fractions. Empirically, binding 72 µg protein to 1.5 µl of beads resulted in approximately 80% of the enzyme remaining immobilized, meaning at least 50 µg (or 600 pmol) protein (Fig. 18/14,15). In terms of stability, the bound enzyme seemed to retain its functional capacity even at room temperature within the timeframe of the library binding incubation and only slightly decreased compared to the free soluble form (Fig. 20). Follow-up elution with 360 mM imidazole was complete, based on repeated elution and SDS-PAGE analysis. Library screening was done as described in the methods section.

By inputting the sequencing data, the analysis portal associated with the compound library's database returned 50 of the 10 million compounds with the highest z-score. There was no documentation provided on how the z-scores were calculated, but they likely come from the same bioinformatics pipeline that was used in (89) by the same company (DyNAbind). In this case, the score is the number of standard deviations the

compound is enriched by, compared to the mean abundance of other library compounds. Based on the large drop in z-score after the 5th compound (Fig. 21), we have chosen the first 5 compounds to function as future leads that will need to be further validated for inhibition.

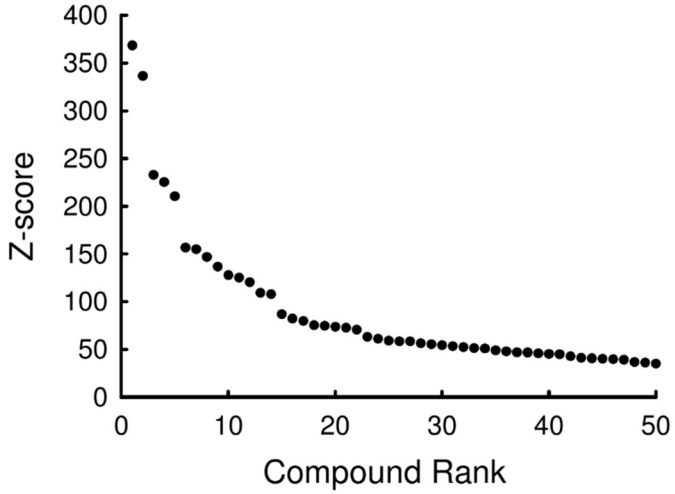

Figure 21, The result from the library screening. The compounds are listed in decreasing rank order with their respective enrichment degree measured in z-score.

5. Discussion

Our major result was highlighting the importance of the electron acceptor in KGDHC mediated substrate-level phosphorylation and possible ways it can be provided. With glutamate and malate, reverse succinate dehydrogenase contribution has been overlooked. Our results suggest that initially the NAD regeneration for KGDHC is mostly dependent on residual aerobic electron transport chain activity, but this is followed by a fumarate dependent phase where the concerted effort of complex I and reverse SDH regenerates the NAD required for KGDHC to provide succinyl-CoA. This also explains why we found complex I inhibition by rotenone detrimental for glutamate-malate fuelled substrate-level phosphorylation in anoxia previously.

Previously, we thought that succinate accumulation was the reason why atpenin was detrimental for substrate-level phosphorylation(49). By the law of mass action, an increase in succinate concentration could make ADP phosphorylation by STK thermodynamically unfavourable. We observed succinate accumulation under control conditions, but did not see it with atpenin (Tabl. 1). Instead, atpenin inhibited substrate-level phosphorylation can be explained by the elimination of SDH's contribution. Kinetically, the reversal of SDH has been debated due to its sluggish fumarate reduction. However, it seems to have been a crucial factor and has been missing from our model of processes involved in substrate-level phosphorylation maintenance. While the project was underway, results from another study using isotope tracers came out, reinforcing the physiological possibility of reverse SDH activity (90). In addition to promoting KGDHC activity, the hydrogen ion translocation by residual complex I activity would also cooperate in membrane potential maintenance. This reduces the necessary rate of ATP hydrolysis by ATP synthase for achieving the same equilibrium membrane potential, preserving ATP for the rest of the cell.

Mutations that impair SDH have been associated with tumorigenesis and pseudohypoxia (91). In such cases of SDH dysfunction, or when succinate accumulation exceeds the transport capacity, MDH2 may provide an alternative way to regenerate NAD for KGDHC. The physiological relevance is questionable since both aspartate and 2-oxoglutarate availability is highly limited compared to glutamine (38, 39). The additional electron pair that comes with the amino group makes glutamate an inferior replacement

for 2-oxoglutarate as well. On the other hand, experimentally this could be a useful approach for specifically addressing how MDH2 contributes to NADH oxidation or how it changes under other conditions of interest. If we compare pure MDH2 (glutamate-aspartate-atpenin) and pure SDH (glutamate-malate) supported substrate-level phosphorylation, our observation is that SDH has a much greater capacity to deal with additional reducing equivalents.

Safranin was not an inert component of our previous experiments. Seemingly, there are two distinct processes at work. Firstly, while excited with continuous light irradiation (which is necessary for membrane potential tracking), safranin can directly react with NADH. This was the dominant process for safranin reduction with permeabilized mitochondria and NADH. Safranin is not the only compound that shows the ability to generate hydrogen peroxide with NADH when excited. Resorufin, the product of resazurin reduction or amplex red oxidation (92), and flavins (93) also showed this property. All of them are fluorescent compounds with condensed aromatic planar structure, so their excited states may have an electron configuration that is similarly favourable for the two-electron transfer. As an exception, flavins do not require light to react with NADH, but photocatalysis does increase the rate of the reaction.

Secondly, with intact mitochondria, the photoinduced reaction seems to be minimal and may not end up altering general experimental results significantly. Yet, there was still measurable safranin reduction in the absence of light. For this case, we were unable to make any definitive conclusions regarding the electron source, we only hypothesise it to be NADH. Our results show that the reduced safranin can be oxidised by SDH, which further underlines its bidirectional nature. Interestingly, when reverse SDH substrates fumarate or malate are present, but SDH is inhibited, there was an intermediate state with a limited increase in electrode current that did not result in a fluorescence decrease over time.

From the perspective of other undesirable properties, the electron mediation does not lead to the previously known decrease of phosphorylating oxygen consumption rate, which has been the major concern (71, 72). However, it could explain the overshadowed increase in „leak" respiration in the presence of NADH-based respiratory substrates (72). Nonetheless, it is advisable to use a different method for membrane potential measurement, for example rhodamine 123, which does not exhibit reduction in anoxia

and has a much better fluorescence quantum efficiency. With rhodamine 123 we have not observed any artificial deviations from the expected results so far.

We found 2-oxobutyrate to be a useful metabolite for adjusting the ATP output of mitochondrial substrate-level phosphorylation. Its metabolism can compete with the 2-oxoglutarate pathway without contributing to net ATP production. This could be used to diminish substrate-level phosphorylation, similar to 3-hydroxybutyrate (94). Compared to 2-oxobutyrate, 3-hydroxybutyrate's mode of action is different. 3-hydroxybutyrate increases the NADH load by its oxidation to acetoacetate, thus decreasing the NAD availability for KGDHC. Because of the alternative attack point, 2-oxobutyrate can even work in a combination with 3-hydroxybutyrate as we saw in the results. This can be particularly useful when 3-hydroxybutyrate alone is insufficient to suppress substrate-level phosphorylation. In these cases, when increasing 3-hydroxybutyrate concentration does not result in observable change, adding 2-oxobutyrate can further lower matrix ATP formation, as indicated by the cATR-induced depolarisation. Considering that it required higher concentrations to have a noticeable effect, the physiologic importance is questionable. The serum concentration of 2-oxobutyrate is very small (41). Only about 10% of threonine was estimated to be metabolised to 2-oxobutyrate in pigs (95), and about 80% of 2-oxobutyrate originates from the homocysteine metabolism (95). It has been proposed that 2-oxobutyrate could also act as an alternative substrate to lactate dehydrogenase, forming 2-hydroxybutanoate to support glycolytic ATP generation (96). Therefore, the net effect of 2-oxobutyrate in whole cells would depend on the balance of its support for cytosolic substrate-level phosphorylation and its opposition for mitochondrial substrate-level phosphorylation.

To directly address substrate-level phosphorylation by STK, we expressed the recombinant human enzyme with the ATP-specific beta subunit. Based on our results, the N-terminal methionine does get cleaved off of the beta subunit by the Escherichia coli methionine aminopeptidase. The methionine retention was described for the GTP-specific subunit starting with Met-Asn-Leu (97). For the ATP-specific subunit we followed Sherley et al. (88) and used Met-Ser-Leu by changing the first leucine into the initiator methionine. Perhaps the difference in the second amino acid is responsible, and the cleavage is allowed before serine but is not allowed before asparagine. Consequently, the best course of action would be to modify the N-terminal in such a way that preserves the

hydrophobic nature of the original leucine, but the replacing amino acid is smaller in size, so that the initiator methionine in front of it remains cleavable. The rule of thumb is that smaller amino acids permit the methionine cleavage (98). Valine insertion between the methionine and serine could be a suitable solution. This turns the native Leu-Ser-Leu sequence into (Met)-Val-Ser-Leu. Valine is a compromise that has a variable cleavage frequency (98), but has the greatest resemblance to leucine. Should valine not produce the desired outcome, the remaining alternatives are either using alanine instead of valine ((Met)-Ala-Ser-Leu) or replacing serine with threonine and keeping the methionine instead of the leucine (Met-Thr-Leu). Since the N-terminal of the beta subunit is not as free as the other terminals, this could have a role in structural integrity or function. Leaving it longer by just adding a methionine to the original sequence is also detrimental to the proper function (97). It cannot be ruled out that this is part of the reason why crystallisation attempts have been unsuccessful so far (99), as well as the reason for the somewhat anomalous reaction kinetic behaviour.

In the literature, we found that various research groups have used very different storage conditions for STK. Fraser et al. (97), Cha et al. (100) and Hsueh et al. (101) stored the enzyme as a suspension in ammonium sulfate. Ammonium sulfate did not improve stability in our experience. In addition, precipitation would risk aggregate formation and could distort library screening results. Baccanari et al. (102) and Hsueh et al. (101) recommended a high glycerol concentration for improved stability without freezing. On the contrary, our enzyme retained its activity better without glycerol. Mazumder et al. (103), Huang et al. (104) and Sherley et al. (88) stored the enzyme frozen with little or no glycerol. Our results were more in line with observations by Cha et al. (100), pointing to an activity loss of 50% for one freeze-thaw cycle without glycerol. Overall, our stability experiments showed a markedly different behaviour for recombinant STK compared to what we found for analogous proteins. We used these results to ensure optimised conditions for the library screening. Because we did not have any previous knowledge of the expected compound binding affinity, we used the highest recommended amount of protein for the screening experiment. Follow-up validation and experiments with our screening hits are in progress, but before any real inhibition is shown no structure-activity relationship can be made. We plan to address them in a new more miniaturised microplate assay format to reduce the required amount of purified enzyme.

6. Conclusions

2-oxobutyrate mediated substrate-level phosphorylation

In contrast to 2-oxoglutarate, the conversion of 2-oxobutyrate to succinyl-CoA involves an additional ATP-requiring step. This negates the ATP yield of mitochondrial substrate-level phosphorylation by STK. The metabolism of 2-oxobutyrate competes with 2-oxoglutarate in isolated mitochondria when added exogenously. This results in the reduction of ATP production under pseudoanoxic conditions, promoting ANT reversal. This interference with substrate-level phosphorylation can be combined with 3-hydroxybutyrate for an additive effect, due to the separate mode of action.

Electron acceptor supply for KGDHC

Substrate-level electron acceptors are crucial in supporting continued operation of KGDHC under anoxia and thereby in providing ATP to prevent ANT reversal. Fumarate, derived from reversible malate dehydration, serves to support reverse SDH and complex I activity coupled by ubiquinone. Oxaloacetate, coming from aspartate transamination uses MDH2 to directly regenerate NAD. Both are sufficient on their own to promote substrate-level phosphorylation under anoxic conditions. Consequently, their absence or abolition would be detrimental for substrate-level phosphorylation and would lead to ATP import by ANT.

We showed that safranin can act as an electron sink when used in the presence of mitochondria. Safranin can be reduced under two separate conditions. One, continuous light excitation in aqueous solution with NADH forms reduced safranin irrespective of mitochondria. Under aerobic conditions, reduced safranin then rapidly oxidises, forming hydrogen peroxide. This occurs only to a small extent with intact mitochondria, possibly due to lower concentrations or lower effective light intensity. Two, independent from the light-induced reaction, mitochondria reduced safranin in the absence of oxygen. We suspect the electron donor to be NADH, based on the non-enzymatic results and the highly negative reduction potential. Since the reaction is extremely slow, unless the experiment is very sensitive to small perturbations, using low concentrations (5 μM) is unlikely to qualitatively alter experimental results. With respect to substrate-level

phosphorylation it is insufficient, since in the absence of other electron acceptors there is no repolarisation following cATR addition.

Direct STK inhibition:

We optimised the storage conditions for recombinant ATP-specific human STK. Using the recombinant enzyme, we screened a 10 million-compound DNA encoded library to identify the ligands with the highest affinity that will serve as leads for future drug development. Further validation and research are underway to determine whether and how their binding results in inhibition.

7. Summary

We investigated 2-oxobutyrate-mediated substrate-level phosphorylation. Using isolated mitochondria, we demonstrated their ability to take up and metabolise exogenous 2-oxobutyrate. Under rotenone-induced pseudoanoxic conditions, we found that 2-oxobutyrate competed with the metabolism of 2-oxoglutarate and decreased the amount to ATP generated by substrate-level phosphorylation in a concentration-dependent way due to the ATP consumption by the propionyl-CoA carboxylase.

We investigated the ability of MDH2 to support substrate-level phosphorylation under SDH inhibition. Oxaloacetate was supplied to the mitochondrial matrix by aspartate transamination. In anoxia, under atpenin inhibition, we found that isolated mitochondria were capable of sufficient NAD regeneration to maintain substrate-level phosphorylation from 2-oxoglutarate and marginally from glutamate. Omitting the MDH2 step by replacing aspartate with malate caused ANT reversal under the same conditions.

We investigated the possibility of SDH reversal functioning as the electron acceptor pathway in anoxia when malate is used as a respiratory co-substrate with isolated mitochondria. Using the combination of stable isotope tracing with GC-MS and mathematical modelling, we found a coordinated effort by KGDHC and SDH that maintained substrate-level phosphorylation. The NAD for KGDHC is regenerated by oxidation through complex I, coupled to fumarate reduction by SDH. Fumarate is provided by the reversible dehydration of malate.

We investigated the potential for safranin to interfere with electron transfer processes in mitochondria. We demonstrated safranin's photoinduced reduction by NADH. Under aerobic conditions, reduced safranin is rapidly oxidised by oxygen and produces hydrogen peroxide. With intact mitochondria, the light-excitation-associated reaction is very little. In the absence of light excitation, intact mitochondria were still capable of reducing safranin. Fumarate and indirectly malate facilitated the oxidation of reduced safranin through SDH. This was sensitive to malonate but not to atpenin with solubilized mitochondria, suggesting the participation of the flavin site.

To find an inhibitor for STK, we first expressed and purified the recombinant ATP-specific human enzyme. We determined the conditions for its stability and then screened a library of 10 million compounds to find the leads with the highest binding affinity.

8. References

1. Vaupel P, Mayer A, Hockel M. Tumor hypoxia and malignant progression. Methods Enzymol. 2004;381:335-354.
2. Gatenby RA, Gillies RJ. Why do cancers have high aerobic glycolysis? Nat Rev Cancer. 2004;4(11):891-899.
3. Kalogeris T, Baines CP, Krenz M, Korthuis RJ. Ischemia/Reperfusion. Compr Physiol. 2016;7(1):113-170.
4. Parmar K, Mauch P, Vergilio JA, Sackstein R, Down JD. Distribution of hematopoietic stem cells in the bone marrow according to regional hypoxia. Proc Natl Acad Sci U S A. 2007;104(13):5431-5436.
5. Wong CC, Kai AK, Ng IO. The impact of hypoxia in hepatocellular carcinoma metastasis. Front Med. 2014;8(1):33-41.
6. Carnell DM, Smith RE, Daley FM, Saunders MI, Bentzen SM, Hoskin PJ. An immunohistochemical assessment of hypoxia in prostate carcinoma using pimonidazole: implications for radioresistance. Int J Radiat Oncol Biol Phys. 2006;65(1):91-99.
7. Nordsmark M, Loncaster J, Chou SC, Havsteen H, Lindegaard JC, Davidson SE, et al. Invasive oxygen measurements and pimonidazole labeling in human cervix carcinoma. Int J Radiat Oncol Biol Phys. 2001;49(2):581-586.
8. Kaanders JH, Wijffels KI, Marres HA, Ljungkvist AS, Pop LA, van den Hoogen FJ, et al. Pimonidazole binding and tumor vascularity predict for treatment outcome in head and neck cancer. Cancer Res. 2002;62(23):7066-7074.
9. Frolova O, Samudio I, Benito JM, Jacamo R, Kornblau SM, Markovic A, et al. Regulation of HIF-1alpha signaling and chemoresistance in acute lymphocytic leukemia under hypoxic conditions of the bone marrow microenvironment. Cancer Biol Ther. 2012;13(10):858-870.
10. Walsh JC, Lebedev A, Aten E, Madsen K, Marciano L, Kolb HC. The clinical importance of assessing tumor hypoxia: relationship of tumor hypoxia to prognosis and therapeutic opportunities. Antioxid Redox Signal. 2014;21(10):1516-1554.
11. Cairns RA, Harris IS, Mak TW. Regulation of cancer cell metabolism. Nat Rev Cancer. 2011;11(2):85-95.

12. Fukuda R, Zhang H, Kim JW, Shimoda L, Dang CV, Semenza GL. HIF-1 regulates cytochrome oxidase subunits to optimize efficiency of respiration in hypoxic cells. Cell. 2007;129(1):111-122.

13. Moreno-Sanchez R, Marin-Hernandez A, Saavedra E, Pardo JP, Ralph SJ, Rodriguez-Enriquez S. Who controls the ATP supply in cancer cells? Biochemistry lessons to understand cancer energy metabolism. Int J Biochem Cell Biol. 2014;50:10-23.

14. Seagroves TN, Ryan HE, Lu H, Wouters BG, Knapp M, Thibault P, et al. Transcription factor HIF-1 is a necessary mediator of the pasteur effect in mammalian cells. Mol Cell Biol. 2001;21(10):3436-3444.

15. Begum HM, Shen K. Intracellular and microenvironmental regulation of mitochondrial membrane potential in cancer cells. WIREs Mech Dis. 2023;15(3):e1595.

16. Gnaiger E, Kuznetsov AV. Mitochondrial respiration at low levels of oxygen and cytochrome c. Biochem Soc Trans. 2002;30(2):252-258.

17. Pajuelo Reguera D, Cunatova K, Vrbacky M, Pecinova A, Houstek J, Mracek T, et al. Cytochrome c Oxidase Subunit 4 Isoform Exchange Results in Modulation of Oxygen Affinity. Cells. 2020;9(2).

18. Dings J, Meixensberger J, Jäger A, Roosen K. Clinical Experience with 118 Brain Tissue Oxygen Partial Pressure Catheter Probes. Neurosurgery. 1998;43(5).

19. Schultheiss R, Leuwer R, Leniger-Follert E, Wassmann H, Wullenweber R. Tissue pO2 of human brain cortex--method, basic results and effects of pentoxifylline. Angiology. 1987;38(3):221-225.

20. Doppenberg EMR, Zauner A, Watson JC, Bullock R, editors. Determination of the Ischemic Threshold for Brain Oxygen Tension. Intracranial Pressure and Neuromonitoring in Brain Injury; 1998 1998//; Vienna: Springer Vienna.

21. Hockel M, Vaupel P. Tumor hypoxia: definitions and current clinical, biologic, and molecular aspects. J Natl Cancer Inst. 2001;93(4):266-276.

22. Cater D, Garattini S, Marina F, Silver I. Changes of oxygen tension in brain and somatic tissues induced by vasodilator and vasoconstrictor drugs. Proceedings of the Royal Society of London Series B Biological Sciences. 1961;155(958):136-157.

23. Erecinska M, Silver IA. Tissue oxygen tension and brain sensitivity to hypoxia. Respir Physiol. 2001;128(3):263-276.

24. Pfaff E, Klingenberg M. Adenine nucleotide translocation of mitochondria. 1. Specificity and control. Eur J Biochem. 1968;6(1):66-79.

25. Junge W, Nelson N. ATP synthase. Annu Rev Biochem. 2015;84:631-657.

26. Di Lisa F, Menabo R, Canton M, Petronilli V. The role of mitochondria in the salvage and the injury of the ischemic myocardium. Biochim Biophys Acta. 1998;1366(1-2):69-78.

27. Campanella M, Parker N, Tan CH, Hall AM, Duchen MR. IF(1): setting the pace of the F(1)F(o)-ATP synthase. Trends Biochem Sci. 2009;34(7):343-350.

28. Campanella M, Casswell E, Chong S, Farah Z, Wieckowski MR, Abramov AY, et al. Regulation of mitochondrial structure and function by the F1Fo-ATPase inhibitor protein, IF1. Cell Metab. 2008;8(1):13-25.

29. Sanchez-Arago M, Formentini L, Martinez-Reyes I, Garcia-Bermudez J, Santacatterina F, Sanchez-Cenizo L, et al. Expression, regulation and clinical relevance of the ATPase inhibitory factor 1 in human cancers. Oncogenesis. 2013;2(4):e46.

30. Solaini G, Sgarbi G, Baracca A. The F1Fo-ATPase inhibitor, IF1, is a critical regulator of energy metabolism in cancer cells. Biochem Soc Trans. 2021;49(2):815-827.

31. Gunter TE, Pfeiffer DR. Mechanisms by which mitochondria transport calcium. Am J Physiol. 1990;258(5 Pt 1):C755-786.

32. Palmieri F, Pierri CL. Mitochondrial metabolite transport. Essays Biochem. 2010;47:37-52.

33. Pfanner N, Craig EA, Meijer M. The protein import machinery of the mitochondrial inner membrane. Trends Biochem Sci. 1994;19(9):368-372.

34. Zorova LD, Popkov VA, Plotnikov EJ, Silachev DN, Pevzner IB, Jankauskas SS, et al. Functional Significance of the Mitochondrial Membrane Potential. Biochemistry (Moscow), Supplement Series A: Membrane and Cell Biology. 2018;12(1):20-26.

35. Chinopoulos C, Gerencser AA, Mandi M, Mathe K, Torocsik B, Doczi J, et al. Forward operation of adenine nucleotide translocase during F0F1-ATPase reversal: critical role of matrix substrate-level phosphorylation. FASEB J. 2010;24(7):2405-2416.

36. Lambeth DO, Tews KN, Adkins S, Frohlich D, Milavetz BI. Expression of two succinyl-CoA synthetases with different nucleotide specificities in mammalian tissues. J Biol Chem. 2004;279(35):36621-36624.

37. Kiss G, Konrad C, Doczi J, Starkov AA, Kawamata H, Manfredi G, et al. The negative impact of alpha-ketoglutarate dehydrogenase complex deficiency on matrix substrate-level phosphorylation. FASEB J. 2013;27(6):2392-2406.

38. Pitkanen HT, Oja SS, Kemppainen K, Seppa JM, Mero AA. Serum amino acid concentrations in aging men and women. Amino Acids. 2003;24(4):413-421.

39. Haerer AF. Citrate and alpha-ketoglutarate in cerebrospinal fluid and blood. Neurology. 1971;21(10):1059-1065.

40. Smith MJ, Taylor KW. Blood pyruvate and alpha-ketoglutarate in normal and diabetic subjects. Br Med J. 1956;2(5000):1035-1038.

41. Koike K, Koike M. Fluorescent analysis of alpha-keto acids in serum and urine by high-performance liquid chromatography. Anal Biochem. 1984;141(2):481-487.

42. Hu CA, Lin WW, Valle D. Cloning, characterization, and expression of cDNAs encoding human delta 1-pyrroline-5-carboxylate dehydrogenase. J Biol Chem. 1996;271(16):9795-9800.

43. Hou Y, Wu G. Nutritionally Essential Amino Acids. Adv Nutr. 2018;9(6):849-851.

44. Jin L, Alesi GN, Kang S. Glutaminolysis as a target for cancer therapy. Oncogene. 2016;35(28):3619-3625.

45. Yang L, Venneti S, Nagrath D. Glutaminolysis: A Hallmark of Cancer Metabolism. Annu Rev Biomed Eng. 2017;19:163-194.

46. Cooper AJL. [10] l-glutamate-l-amino acid transaminases. Methods in Enzymology. 113: Academic Press; 1985. p. 63-65.

47. Smith EL, Austen BM, Blumenthal KM, Nyc JF. 5 Glutamate Dehydrogenases. In: Boyer PD, editor. The Enzymes. 11: Academic Press; 1975. p. 293-367.

48. Sheu KF, Blass JP. The alpha-ketoglutarate dehydrogenase complex. Ann N Y Acad Sci. 1999;893:61-78.

49. Kiss G, Konrad C, Pour-Ghaz I, Mansour JJ, Nemeth B, Starkov AA, et al. Mitochondrial diaphorases as NAD(+) donors to segments of the citric acid cycle that support substrate-level phosphorylation yielding ATP during respiratory inhibition. FASEB J. 2014;28(4):1682-1697.

50. Paxton R, Scislowski PW, Davis EJ, Harris RA. Role of branched-chain 2-oxo acid dehydrogenase and pyruvate dehydrogenase in 2-oxobutyrate metabolism. Biochem J. 1986;234(2):295-303.

51. Wongkittichote P, Ah Mew N, Chapman KA. Propionyl-CoA carboxylase - A review. Mol Genet Metab. 2017;122(4):145-152.

52. Mazumder R, Sasakawa T, Kaziro Y, Ochoa S. Metabolism of propionic acid in animal tissues. IX. Methylmalonyl coenzyme A racemase. J Biol Chem. 1962;237:3065-3068.

53. Zu Y, Shannon RJ, Hirst J. Reversible, electrochemical interconversion of NADH and NAD+ by the catalytic (Ilambda) subcomplex of mitochondrial NADH:ubiquinone oxidoreductase (complex I). J Am Chem Soc. 2003;125(20):6020-6021.

54. Hakala MT, Glaid AJ, Schwert GW. Lactic dehydrogenase. II. Variation of kinetic and equilibrium constants with temperature. J Biol Chem. 1956;221(1):191-209.

55. Guynn RW, Gelberg HJ, Veech RL. Equilibrium constants of the malate dehydrogenase, citrate synthase, citrate lyase, and acetyl coenzyme A hydrolysis reactions under physiological conditions. J Biol Chem. 1973;248(20):6957-6965.

56. Weinberg JM, Venkatachalam MA, Roeser NF, Nissim I. Mitochondrial dysfunction during hypoxia/reoxygenation and its correction by anaerobic metabolism of citric acid cycle intermediates. Proc Natl Acad Sci U S A. 2000;97(6):2826-2831.

57. Hochachka PW, Dressendorfer RH. Succinate accumulation in man during exercise. Eur J Appl Physiol Occup Physiol. 1976;35(4):235-242.

58. Sanadi DR, Fluharty AL. On the Mechanism of Oxidative Phosphorylation. Vii. The Energy-Requiring Reduction of Pyridine Nucleotide by Succinate and the Energy-Yielding Oxidation of Reduced Pyridine Nucleotide by Fumarate. Biochemistry. 1963;2:523-528.

59. Hochachka PW, Owen TG, Allen JF, Whittow GC. Multiple end products of anaerobiosis in diving vertebrates. Comp Biochem Physiol B. 1975;50(1):17-22.

60. Hirst J, Sucheta A, Ackrell BAC, Armstrong FA. Electrocatalytic voltammetry of succinate dehydrogenase: Direct quantification of the catalytic properties of a complex electron-transport enzyme. Journal of the American Chemical Society. 1996;118(21):5031-5038.

61. Cecchini G, Schroder I, Gunsalus RP, Maklashina E. Succinate dehydrogenase and fumarate reductase from Escherichia coli. Biochim Biophys Acta. 2002;1553(1-2):140-157.

62. Tomitsuka E, Kita K, Esumi H. Regulation of succinate-ubiquinone reductase and fumarate reductase activities in human complex II by phosphorylation of its flavoprotein subunit. Proc Jpn Acad Ser B Phys Biol Sci. 2009;85(7):258-265.

63. Ajalla Aleixo MA, Rangel VL, Rustiguel JK, de Padua RAP, Nonato MC. Structural, biochemical and biophysical characterization of recombinant human fumarate hydratase. FEBS J. 2019;286(10):1925-1940.

64. Ponti V, Dianzani MU, Cheeseman K, Slater TF. Studies on the reduction of nitroblue tetrazolium chloride mediated through the action of NADH and phenazine methosulphate. Chem Biol Interact. 1978;23(3):281-291.

65. Prince RC, Linkletter SJ, Dutton PL. The thermodynamic properties of some commonly used oxidation-reduction mediators, inhibitors and dyes, as determined by polarography. Biochim Biophys Acta. 1981;635(1):132-148.

66. Stiehler RD, Chen T-T, Clark WM. Studies on Oxidation—Reduction. XVIII. Simple Safranines. Journal of the American Chemical Society. 1933;55(3):891-907.

67. Salomi BSB, Mitra CK, Gorton L. Electrochemical and spectrophotometric studies on dyes and proteins labelled with dyes. Synthetic Metals. 2005;155(2):426-429.

68. Ohnishi T, King TE, Salerno JC, Blum H, Bowyer JR, Maida T. Thermodynamic and electron paramagnetic resonance characterization of flavin in succinate dehydrogenase. J Biol Chem. 1981;256(11):5577-5582.

69. Sled VD, Rudnitzky NI, Hatefi Y, Ohnishi T. Thermodynamic analysis of flavin in mitochondrial NADH:ubiquinone oxidoreductase (complex I). Biochemistry. 1994;33(33):10069-10075.

70. Harris EJ, Baum H. Uptake of safranine by cardiac mitochondria. Competition with calcium ions and dependence on anions. Biochem J. 1980;192(2):551-557.

71. Zanotti A, Azzone GF. Safranine as membrane potential probe in rat liver mitochondria. Arch Biochem Biophys. 1980;201(1):255-265.

72. Krumschnabel G, Eigentler A, Fasching M, Gnaiger E. Use of safranin for the assessment of mitochondrial membrane potential by high-resolution respirometry and fluorometry. Methods Enzymol. 2014;542:163-181.

73. Valle VG, Pereira-da-Silva L, Vercesi AE. Undesirable feature of safranine as a probe for mitochondrial membrane potential. Biochem Biophys Res Commun. 1986;135(1):189-195.

74. Rich PR, Mischis LA, Purton S, Wiskich JT. The sites of interaction of triphenyltetrazolium chloride with mitochondrial respiratory chains. FEMS Microbiol Lett. 2001;202(2):181-187.

75. Sevcik P, Dunford HB. Kinetics of the oxidation of NADH by methylene blue in a closed system. The Journal of Physical Chemistry. 1991;95(6):2411-2415.

76. Crane FL, Barr R. [220] Determination of ubiquinones. Methods in Enzymology. 18: Academic Press; 1971. p. 137-165.

77. Komlodi T, Tretter L. Methylene blue stimulates substrate-level phosphorylation catalysed by succinyl-CoA ligase in the citric acid cycle. Neuropharmacology. 2017;123:287-298.

78. Entzeroth M, Flotow H, Condron P. Overview of high-throughput screening. Curr Protoc Pharmacol. 2009;Chapter 9:Unit 9 4.

79. Kleiner RE, Dumelin CE, Liu DR. Small-molecule discovery from DNA-encoded chemical libraries. Chem Soc Rev. 2011;40(12):5707-5717.

80. Smith PK, Krohn RI, Hermanson GT, Mallia AK, Gartner FH, Provenzano MD, et al. Measurement of protein using bicinchoninic acid. Anal Biochem. 1985;150(1):76-85.

81. Akerman KE, Wikstrom MK. Safranine as a probe of the mitochondrial membrane potential. FEBS Lett. 1976;68(2):191-197.

82. Chinopoulos C, Adam-Vizi V. Mitochondrial Ca2+ sequestration and precipitation revisited. FEBS J. 2010;277(18):3637-3651.

83. Laemmli UK. Cleavage of structural proteins during the assembly of the head of bacteriophage T4. Nature. 1970;227(5259):680-685.

84. Bui D, Ravasz D, Chinopoulos C. The Effect of 2-Ketobutyrate on Mitochondrial Substrate-Level Phosphorylation. Neurochem Res. 2019;44(10):2301-2306.

85. Ravasz D, Bui D, Nazarian S, Pallag G, Karnok N, Roberts J, et al. Residual Complex I activity and amphidirectional Complex II operation support glutamate catabolism through mtSLP in anoxia. Sci Rep. 2024;14(1):1729.

86. Votyakova TV, Reynolds IJ. Detection of hydrogen peroxide with Amplex Red: interference by NADH and reduced glutathione auto-oxidation. Arch Biochem Biophys. 2004;431(1):138-144.

87. Lowry OH, Passonneau JV, Rock MK. The Stability of Pyridine Nucleotides. Journal of Biological Chemistry. 1961;236(10):2756-2759.

88. Sherley KR. X-ray crystallography, nucleotide binding, and kinetic studies of human atp-specific succinyl-coa synthetase [Master's thesis]: University of Calgary; 2008.

89. Iqbal S, Jiang W, Hansen E, Aristotelous T, Liu S, Reidenbach A, et al. Evaluation of DNA encoded library and machine learning model combinations for hit discovery. npj Drug Discovery. 2025;2(1):5.

90. Spinelli JB, Rosen PC, Sprenger HG, Puszynska AM, Mann JL, Roessler JM, et al. Fumarate is a terminal electron acceptor in the mammalian electron transport chain. Science. 2021;374(6572):1227-1237.

91. Frezza C, Gottlieb E. Mitochondria in cancer: not just innocent bystanders. Semin Cancer Biol. 2009;19(1):4-11.

92. Zhao B, Ranguelova K, Jiang J, Mason RP. Studies on the photosensitized reduction of resorufin and implications for the detection of oxidative stress with Amplex Red. Free Radic Biol Med. 2011;51(1):153-159.

93. Radda GK, Calvin M. Chemical and Photochemical Reductions of Flavin Nucleotides and Analogs. Biochemistry. 1964;3:384-393.

94. Ravasz D, Kacso G, Fodor V, Horvath K, Adam-Vizi V, Chinopoulos C. Reduction of 2-methoxy-1,4-naphtoquinone by mitochondrially-localized Nqo1 yielding NAD(+) supports substrate-level phosphorylation during respiratory inhibition. Biochim Biophys Acta Bioenerg. 2018;1859(9):909-924.

95. Ballevre O, Cadenhead A, Calder AG, Rees WD, Lobley GE, Fuller MF, et al. Quantitative partition of threonine oxidation in pigs: effect of dietary threonine. Am J Physiol. 1990;259(4 Pt 1):E483-491.

96. Sullivan LB, Gui DY, Hosios AM, Bush LN, Freinkman E, Vander Heiden MG. Supporting Aspartate Biosynthesis Is an Essential Function of Respiration in Proliferating Cells. Cell. 2015;162(3):552-563.

97. Fraser ME, Hayakawa K, Hume MS, Ryan DG, Brownie ER. Interactions of GTP with the ATP-grasp domain of GTP-specific succinyl-CoA synthetase. J Biol Chem. 2006;281(16):11058-11065.

98. Wingfield PT. N-Terminal Methionine Processing. Curr Protoc Protein Sci. 2017;88:6 14 11-16 14 13.

99. Huang J, Fraser ME. Structural studies of human ATP-specific succinyl-CoA synthetase. Acta Crystallographica Section A. 2018;74(a1):a135.

100. Cha S, Cha CJ, Parks RE, Jr. Succinic thiokinase. IV. Improved method of purification, arsenolysis of guanosine triphosphate, succinate-dependent guanosine triphos- phatase activity, and some other properties of the enzyme. J Biol Chem. 1967;242(11):2577-2581.

101. Hsueh S-C, Pan L-Y, Lee M-C, Lee A-C. Purification and Characterization of Succinyl Thiokinase from Pig Heart. Journal of Marine Science and Technology. 2013;21(4):14.

102. Baccanari DP, Cha S. Succinate thiokinase. VI. Multiple interconvertible forms of the enzyme. J Biol Chem. 1973;248(1):15-24.

103. Mazumder R, Sanadi DR, Rodwell VW. Purification and properties of hog kidney succinic thiokinase. J Biol Chem. 1960;235:2546-2550.

104. Huang J, Fraser ME. Tartryl-CoA inhibits succinyl-CoA synthetase. Acta Crystallogr F Struct Biol Commun. 2020;76(Pt 7):302-308.

9. Bibliography of the candidate's publications

Related publications:

1. Ravasz D, Bui D, Nazarian S, Pallag G, Karnok N, Roberts J, et al. Residual Complex I activity and amphidirectional Complex II operation support glutamate catabolism through mtSLP in anoxia. Sci Rep. 2024;14(1):1729.
2. Bui D, Ravasz D, Chinopoulos C. The Effect of 2-Ketobutyrate on Mitochondrial Substrate-Level Phosphorylation. Neurochem Res. 2019;44(10):2301-2306.

Unrelated publications:

1. Doczi J, Karnok N, Bui D, Azarov V, Pallag G, Nazarian S, et al. Viability of HepG2 and MCF-7 cells is not correlated with mitochondrial bioenergetics. Sci Rep. 2023;13(1):10822.
2. Pallag G, Nazarian S, Ravasz D, Bui D, Komlodi T, Doerrier C, et al. Proline Oxidation Supports Mitochondrial ATP Production When Complex I Is Inhibited. Int J Mol Sci. 2022;23(9).
3. Szabo E, Wilk P, Nagy B, Zambo Z, Bui D, Weichsel A, et al. Underlying molecular alterations in human dihydrolipoamide dehydrogenase deficiency revealed by structural analyses of disease-causing enzyme variants. Hum Mol Genet. 2019;28(20):3339-3354.

10. Acknowledgements

I would like to thank Dr. Christos Chinopoulos for leading me as a principal investigator, providing the funding for the research and letting me work independently.
I would like to thank the rest of the research group Dr. Dóra Ravasz, Dr. Gergely Pallag, Noémi Karnok, Dr. Judit Dóczi, Dr. Sara Nazarian for continuous discussions, collaborations, instructions, help and support.
I would like to thank Dr. Krisztina Paál for the codon optimisation of recombinant STK.
I would like to thank Dr. Eszter Szabó and Dr. Attila Ambrus for discussions related to KGDHC and for introducing me into research.
I would like to thank Dr. Jennie Roberts, Dr. Bryan P. Marzullo, Prof. Daniel A. Tennant for the GC-MS metabolite quantification.
I would like to thank Prof. Attila Patócs, Dr. Anikó Bozsik, Dr. Tímea Pócza for the qPCR, PCR and NextGen sequencing of the DNA-encoded library.
I would like to thank Dr. Iordanov Iordán for consultations with recombinant expression, for the competent BL21(DE3) cells and for access to his group's infrastructure.
I would like to thank Dr. Olivér Ozohanics for the mass spectrometric quality analysis of the recombinant STK and for access to the vacuum centrifuge.
I would like to thank Oroboros Instruments GmbH for the opportunity to test the Q-module of the NextGen-O2k instrument.
A mention of gratitude for M. Wayne Davis for the freely available ApE software that was used to design the plasmid.
Another mention of gratitude for the publicly available NIST Uncertainty Machine v1.5 for error propagation calculations.